Coupling of H vibration to substrate electronic states in Mo(100)-$p(1\times1)$H and W(100)-$p(1\times1)$H: Example of strong breakdown of adiabaticity

J. E. Reutt, Y. J. Chabal, and S. B. Christman
AT&T Bell Laboratories, Murray Hill, New Jersey 07974-2070
(Received 2 February 1988; revised manuscript received 26 April 1988)

The surface infrared reflectance spectra of Mo(100)-$p(1\times1)$H and W(100)-$p(1\times1)$H are both characterized by two vibrational absorptions in the 800–4000-cm^{-1} region—a broad band at 1016 cm^{-1} at $T=100$ K for H on Mo(100) and at 1069 cm^{-1} at $T=300$ K for H on W(100), corresponding to the symmetric stretch (ν_1), and a narrow derivative-like feature at 1302 cm^{-1} on Mo(100) and at 1269 cm^{-1} on W(100), identified as the first overtone of the wag motion ($2\nu_2$). The physical origin of the line shapes, as well as the larger intensity of the $2\nu_2$ than expected from adiabatic considerations, were investigated through phenomenological line-shape analysis of data obtained as a function of temperature and relative H/D and H/CO coadsorption concentrations. Inhomogeneous broadening is negligible, and dephasing processes contribute weakly to both ν_1 and $2\nu_2$ linewidths. The most distinctive feature of the spectra, the derivative or "Fano shape" of $2\nu_2$, arises from a nonadiabatic coupling between the sharp $2\nu_2$ vibration and the continuum absorption due to surface electronic transitions. The asymmetry parameter $\tilde{\nu}_0\tilde{\tau}$, which gauges the $2\nu_2$-continuum coupling strength, is temperature insensitive and does not exhibit an isotopic dependence, as predicted for a strong breakdown of adiabaticity. The narrow linewidths observed for $2\nu_2$ on both surfaces at $T=100$ K, 12.2 cm^{-1} on Mo(100) and 18.5 cm^{-1} on W(100), set a limit on the lifetime of these vibrational levels at $T_1\geq0.9$ ps and $T_1\geq0.6$ ps, respectively. Direct evidence for the electronic excitation continuum that interacts with $2\nu_2$ is obtained by analyzing changes in broadband reflectivity measurements on W(100)/H and Mo(100)/H as a function of coverage. Both H-saturated surfaces exhibit a strong absorption with x-y symmetry that can be related to optical excitation of surface states. Further support for surface-state participation in the nonadiabatic process is inferred from the strong attenuation of the $2\nu_2$ intensity upon CO co-adsorption.

I. INTRODUCTION

Hydrogen-covered transition-metal surfaces serve as the prototypical metal-adsorbate systems in surface science. Although the relative simplicity of these systems has prompted considerable experimental[1] and theoretical[2] work, many questions remain. On W(100) and Mo(100), in particular, the dynamics and energetics of these two open-lattice surfaces are sufficiently subtle to produce a series of H-induced surface phases with different phase transitions,[3–10] despite the structural similarities between these two surfaces. At saturation coverage, however, both surfaces exhibit well-defined (1×1) low-energy electron diffraction (LEED) patterns with simple geometries. The present study utilizes infrared-reflection absorption spectroscopy (IRRAS) to investigate in detail the vibrational and electronic properties of these two (1×1) phases over the 800–4000-cm^{-1} region.

Since hydrogen presents a low-scattering cross section for electrons and ions, the usually powerful LEED, surface-extended x-ray-absorption fine-structure (SEXAFS), and ion-scattering techniques cannot provide definitive information concerning the hydrogen absorption sites and local geometries. In contrast, surface hydrogen is easily accessible to vibrational spectroscopy. In fact, the original site assignment of W(100)-$p(1\times1)$H, to H occupying a twofold bridge site on the C_{4v} tungsten surface atoms, was based upon the electron-energy-loss–spectroscopy (EELS) data of Ho, Willis, and Plummer.[11] Dipole and impact scattering spectra were used to identify all the normal modes of the bridge-bonded hydrogen: the symmetric stretch (ν_1), wag (ν_2), and asymmetric stretch (ν_3). For Mo(100)-$p(1\times1)$H, only dipole EELS results have been reported[12] and the adsorbate location is not determined unambiguously.

Surface infrared spectroscopy (SIRS) is a complementary vibrational spectroscopy to EELS since it offers higher resolution (typically 1 cm^{-1} compared to ~50 cm^{-1} in EELS), rigorous dipole selection rules, and similar sensitivity in the 800–5000-cm^{-1} spectral range. It also probes the surface and near-surface electronic response according to well-understood mechanisms: free-electron scattering and optical transitions (intraband or interband). Therefore, in addition to the structural information derived from the precise frequencies of dipole-active modes associated with specific phases, dynamical information can, in principle, be inferred through the details of the vibrational line shapes and changes in broadband electronic reflectivity. In fact, it has been argued[13–22] that phenomenological line-shape analysis, based upon a formal theory of the interaction of electromagnetic radiation and solid surfaces, can provide experimentally accessible information concerning the interaction of the adsorbate vibrations with the substrate electrons on a picosecond time scale.

Recent surface infrared studies[23,24] have revealed that

two distinct dipole-active vibrational absorptions characterize the W(100)-$p(1\times1)$H system, a broad band at 1069 cm^{-1}, which was also observed by EELS and assigned to the symmetric stretch mode, and a sharp asymmetric feature at 1269 cm^{-1}, which was not detected in specular EELS.[11,25–29] In the present study, we find that the Mo(100)-$p(1\times1)$H phase is also characterized by two dipole-active modes: a broad band at 1016 cm^{-1}, as observed by EELS,[12] and a sharp asymmetric feature at 1302 cm^{-1}, which was not evident in the specular EELS study. The identity and excitation origin of this feature are the central questions addressed in this paper. We show that, as in the case of W(100), this band can be assigned to the first overtone of the wag mode ($2\nu_2$) and that it appears to be enhanced due to nonadiabatic coupling to the substrate electronic structure. In addition, we show direct evidence for such surface-electronic absorption at saturation coverage on these two surfaces.

Since specular EELS and SIRS are presumed to yield identical information, the observation of this sharp asymmetric feature by SIRS and its absence from EELS measurements cannot be dismissed. In most documented studies of adsorbates on metal surfaces, the strength of the dynamic dipole or effective charge (e^*/e) extracted from both techniques is identical.[30] The differing sensitivities of EELS and SIRS to the hydrogen $2\nu_2$ phonon on Mo(100) and W(100) offer a clue to the physical origin of its dipole activity.

SIRS and specular EELS can be contrasted by the magnitude of the parallel momentum ($Q_\parallel$) associated with their vibrational excitation and by the nature of their electronic losses (or absorption). The $Q_\parallel$ imparted in an EELS experiment ($\sim10^6$ cm^{-1}) is considerably larger than that associated with photons ($\sim10^3$ cm^{-1}). However, both values are very small with respect to the Brillouin zone ($Q_\parallel^{BZ}\sim10^8$ cm^{-1}) and their difference is only important in cases where dispersion crossing occurs at very low $Q_\parallel$ values.[31] We show, in fact, that in the case of H on Mo(100) or W(100) such a mechanism is not operative.

On the other hand, the electronic excitation within the substrate is different depending on the probe. In the case of SIRS, the fields inside the substrate are primarily tangential to the surface and decay exponentially within the skin depth ($\delta\sim150$ Å for W). Therefore, only the tangential component of the substrate response $\epsilon_\parallel$ is probed.[1] In contrast, in specular scattering, low-energy electrons primarily excite transitions with normal symmetry over a depth $\Delta\sim Q_\parallel^{-1}$ (~90 Å for 3-eV electrons and 0.16-eV loss). Thus, only the normal component of the substrate response, $\epsilon_\perp$, is probed. Experimental determination of the differences in the broadband electronic absorption can therefore help to elucidate the nature of the surface electron absorption.

Accordingly, reflectivity changes for the Mo(100) and W(100) surfaces at various stages of H adsorption were measured to identify contributions by free-carrier excitations to the infrared spectra. In particular, the presence of surface-electronic states that can couple to the vibrational modes were inferred with this technique. Since the reflectivity variations due to broadband absorption are found to be generally much larger than those due to pure vibrational features, the possibility for intensity borrowing by a vibrational mode, e.g., the $2\nu_2$ mode, via a nonadiabatic coupling to electronic states near the Fermi level is possible. We argue, furthermore, that the observation of the $2\nu_2$ feature *requires* the detection of these electronic transitions.

The influence of surface electronic states in the H vibrational spectra was also investigated through H/CO co-adsorption studies at saturation coverage on Mo(100), since CO can modify the surface electronic structure. The line-shape parameters of the $2\nu_2$ mode were monitored as a function of H partial coverage, with CO occupying the rest of the surface. A strong attenuation of the $2\nu_2$ intensity by small amounts of CO corroborates the proposal that coupling to surface-electronic states is responsible for the enhanced absorption of the $2\nu_2$ mode.

This paper is organized as follows. Section II describes the main experimental procedures. Section III is devoted to the details of the line-shape analysis. The experimental results are reported in Sec. IV, which includes a summary of the low-coverage phases relevant to the study of the saturation phase (Sec. IV A), the spectroscopy of the pure phases (Sec. IV B), the temperature dependence of the pure phases (Sec. IV C), the H/D co-adsorption results (Sec. IV D), the broadband reflectivity results (Sec. IV E), and data concerning H/CO coadsorption (Sec. IV F). The interpretation of these results appear in Sec. V. Finally, the principal conclusions are drawn in Sec. VI.

II. EXPERIMENT

The experimental apparatus is similar to that described in Ref. 8. Briefly, it consists of an ultrahigh-vacuum (UHV) chamber, variable-temperature sample manipulator, a Michelson interferometer, Hg-Cd-Te detectors, appropriate reflective optics, video rear-view low-energy electron diffraction, and a cylindrical-mirror-analyzer (CMA) Auger-electron spectrometer (AES). The main differences between the experimental methods for Mo(100)-$p(1\times1)$H and W(100)-$p(1\times1)$H involve details of sample preparation and methodology for data acquisition. The vibrational modes of H of Mo(100) are weaker than on W(100), necessitating more signal averaging. Also, owing to a lower desorption temperature for H from Mo(100) than from W(100) most of the runs were taken at $T=100$ K for the Mo(100)/H system and at $T=300$ K for the W(100)/H system, making it difficult to use the reflectivity of the clean Mo(100) surface as a reference.

The Mo(100) sample ($3.0\times0.5\times0.2$ cm^3) was cut within 1° of the (100) face and polished by Scientific International Inc., New Jersey.[32] The experimental geometry afforded concurrent infrared and LEED measurements. Before mounting the sample into the UHV system, a type-*C* (W–Re 5 at. % versus W–Re 26 at. %) thermocouple was spot welded onto the side of the sample. The temperature could be measured within an accuracy of 10° over the 80–2500-K range. An optical pyrometer was also employed to cross check temperatures over the 1100–2500-K range. The Mo(100) sample was cleaned

initially by cycles of baking in 10^{-7} torr of O_2 (> 10 h total) and flashing in vacuum to 2050 K. After most of the carbon originating from the bulk had been removed, cleaning was restricted to high-temperature flashes only (2050 K in 3×10^{-10} torr vacuum), prior to each individual run, to avoid the CO contamination of the vacuum that inevitably follows an oxygen bake.

The base pressure was 1.5×10^{-10} torr during most infrared measurements, the dominant residual gas being hydrogen. As a result, it was impossible to keep the cold surface completely free of hydrogen. Since the sample was heated by electron bombardment, the thermal conduction to the holder was minimized and the time required for the sample to cool to 100 from 2050 K was 15 min. Isothermal experiments could not, therefore, be performed using the clean Mo(100) surface as a reference. In fact, it was found that 25 min were required after the flash for the system to stabilize fully so that reflectances with optimal baselines could be measured.

As indicated previously,[8] the position of the H_2 and D_2 leak valves with respect to the UHV gauge and the sample were such that the uncorrected exposures quoted in this paper are 10–20% high. The coverage calibrations are determined for the present study by using the LEED patterns and the associated coverages established by Prybyla *et al.*,[33] which assume that the saturation coverage is two H atoms per Mo surface atoms, as has been determined for W(100). This point will be addressed further in Sec. IV A.

For the Mo(100) experiment, three masses could be monitored simultaneously during thermal desorption experiments so that the relative coverage of H and D could be measured accurately in isotopic mixture experiments, even though the mass spectrometer was not positioned in line of sight of the sample. This was not the case in the W(100) study, for which only one mass could be monitored for a given thermal desorption spectrum.

The purity of the sample was determined with AES initially. The carbon (271-eV) and oxygen (503-eV) *KLL* signal levels were $<0.1\%$ of the Mo *MNN* (186-eV) level. During actual experiments, however, the development of specific LEED patterns was found to be a more sensitive test of the surface purity. For instance, the observation of the $Ic(2\times2)$ pattern below $T=200$ K, characteristic of the clean Mo(100) surface,[9,10,33] was the best indication that the surface contamination was negligible and the chamber base pressure adequate for studying hydrogen and/or deuterium adlayers. For room-temperature runs this criterion could not be used since the clean Mo(100) LEED pattern is (1×1). However, the contamination at $T=300$ K is generally less of a problem than at $T=100$ K due to lower sticking coefficients for adspecies.

The Mo(100) surface exhibits a number of well-defined LEED patterns as hydrogen is adsorbed that vary as a function of both coverage and temperature. Recently, these phases have been the subject of an extensive study.[9,10,33] For the reader's convenience the H/Mo(100) T-Θ phase diagram of Ref. 9 is reproduced in Fig. 1. Associated with each phase are specific vibrational and electronic absorptions. The wave numbers of the vibrational bands are shown in boldface in Fig. 1. The electronic

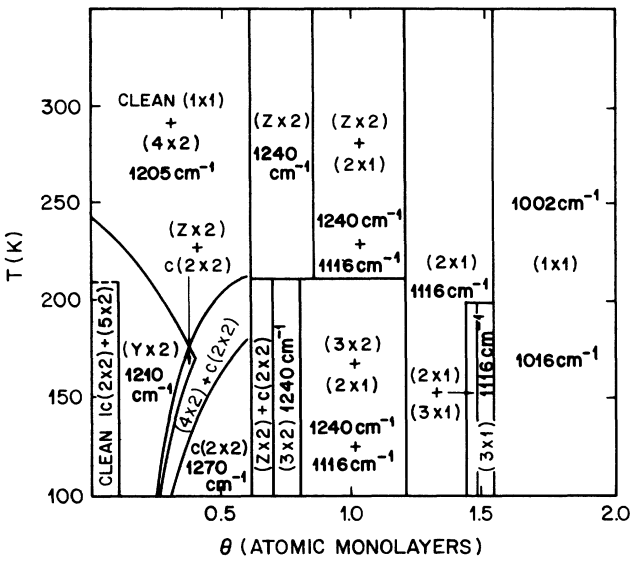

FIG. 1. Phase diagram (T-Θ) for H chemisorption on Mo(100) up to saturation coverage ($\Theta=2$ ML), reproduced from Ref. 9. The $(y\times2)$ and $(z\times2)$ phases refer to surface phases that are continuously variable with coverage and temperature ($y=5\rightarrow4$, $z=4\rightarrow3$).

contribution is manifested as a broadband absorption over the 800–5000-cm^{-1} range of investigation.

Quantitative measurements of the change in electronic absorption as a function of coverage require good thermal stability throughout the measurements because this electronic absorption is a strong function of temperature.[34] Furthermore, the sample positional stability, which is also sensitively monitored by the infrared (ir) spectrum, was not achieved until the temperature of the sample had reached a constant level for several minutes. Consequently, systematic errors arising from the finite thermal and positional stability of the sample limited the accuracy of the absolute reflectance measurements to $\Delta R/R\sim10^{-4}$.

The necessity for sample stability is illustrated in Figs. 2(a)–2(c), where the reflectance of the saturation phase, Mo(100)-(1×1)H, is plotted using different reference phases. The reflectance is defined as the ratio of two reflectivities R/R_0, R being for the phase under study and R_0 for the reference phase. A recorded reflectivity spectrum is a convolution of the actual metal-adsorbate reflectivity spectrum and the instrument response, which is determined by a variety of factors including the source-emission spectrum, the absorption by the reflective optics, the efficiency of the beam splitter, the window transmission, and the detector response. A typical reflectivity spectrum is shown in Fig. 2(d). The instrument response is effectively removed by "ratioing" the metal-adsorbate reflectivity spectrum to a reference-metal reflectivity spectrum. However, several features characteristic of the instrument response appear when the system is unstable or the instrument response function is not adequately removed. This effect can be seen in Figs. 2(b) and 2(c). Because the temperatures of the reference surfaces are higher than that of the (1×1) surface,

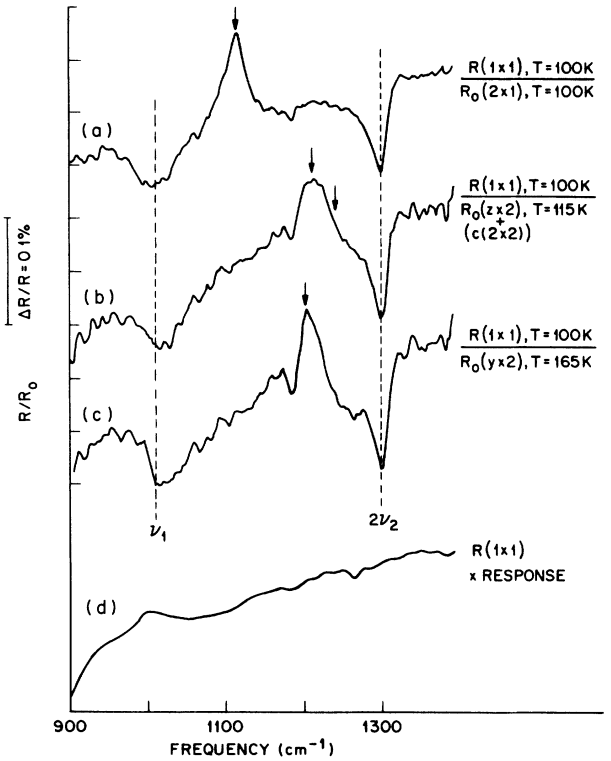

FIG. 2. Reflectance spectra ($\Delta R/R_0$) for Mo(100)-$p(1\times1)$H for several reference phases (R_0): (a) $R_0=(2\times1)$ at $T=100$ K; (b) $R_0=(z\times2)+[c(2\times2)]$ at $T=115$ K $(4<z<3)$; and (c) $R_0=(y\times2)$ $(5<y<4)$ at $T=165$ K. The raw reflectivity of the (1×1) phase, which includes the system response, is given in (d). Arrows pointing to positive going reflectivity changes indicate vibrational absorption of the reference phase (R_0). Note that thermal instability introduces spectral artifacts in the reflectance due to inadequate filtering of the system response.

spectral signatures from the instrument response manifested in Fig. 2(d) (the sharp feature at 1250 cm^{-1} and the dip below 1000 cm^{-1}) are increasingly evident in Figs. 2(b) and 2(c). Such systematic artifacts may be reproduced by monitoring H-saturated Mo(100) (i.e., under finite H partial pressure) as the sample cools and the system stabilizes. A spectral artifact around 1700 cm^{-1} (not shown) was found to be most sensitive to the overall stability of the system and was used as the best measure of the data quality.

A major concern for the spectroscopy of Mo(100)-$p(1\times1)$H was, therefore, to eliminate these systematic problems. A practical solution was to use the (2×1) phase observed at $\Theta=1.3$ monolayers (ML), which is the ordered phase immediately preceding the (1×1) phase, as a reference for the (1×1) phase. For broadband studies of the electronic absorption, the lowest-coverage phase we were able to use reliably as a reference was the $c(2\times2)$ phase at $\Theta=0.5$ ML and for $T<200$ K.

III. LINE-SHAPE ANALYSIS

Spectral line shapes can be a source of information concerning the pathways and rates of energy transfer between the adsorbate phonons and the substrate. Vibrational lifetime information can frequently be obscured, however, by other contributions to the spectral line shape, e.g., surface inhomogeneities and vibrational dephasing effects. In order to investigate the physical origin of the recorded line shapes, it is necessary first to quantify the measured line shape. This is best accomplished through linear least-squares-fitting procedures that utilize formal vibrational and background line-shape functions. Reflectance profiles can then be monitored as a function of surface temperature, sample-preparation conditions, and adlayer composition to determine the various contributions to the overall spectral line shapes.

For metal substrates, in particular, infrared absorption due to free-carrier scattering and interband or intraband transitions taking place at or near the surface can provide a non-negligible frequency-dependent background to the recorded infrared reflectance spectrum if this absorption changes upon H adsorption. Since this background is an electronic continuum upon which the discrete adsorbate vibrational spectrum is embedded, a realistic treatment of the "vibrational line shape" must consider the contributions of this background. This is particularly important for cases where significant electronic damping of the adlayer vibrations is occurring, since part of the background can interact strongly with the adsorbate motion.

The infrared vibrational line shapes of Mo(100)-$p(1\times1)$H and W(100)-$p(1\times1)$H were studied by fitting the infrared region of interest to characteristic spectral forms—Gaussian, Lorentzian, and generalized (Fano) functions—and including electronic broadband absorption in the fits as a power series of frequency. Although inhomogeneous broadening may result in complicated line shapes,[20] a Gaussian line shape is generally indicative of an inhomogeneity-dominated line shape and is of the form

$$L_G(\tilde{\nu})\equiv\Delta R/R_0\sim e^{(\tilde{\nu}-\tilde{\nu}_0)^2/\gamma^2}, \tag{1}$$

where $\tilde{\nu}$ is the probing radiation energy (in cm^{-1}), $\tilde{\nu}_0$ is the mean phonon wave number, and γ is the peak full width at half maximum (in cm^{-1}), establishing an upper bound for the natural linewidth of the phonon.

A Lorentzian form has typically been associated with various damping (T_1) and vibrational decay (T_2) mechanisms.[19] It is obtained simply by solving the equations of motion of a layer of dipoles, subject to damping, yielding the generalized susceptibility function

$$\alpha=-\mu^2(2\tilde{\nu}_0)/(\tilde{\nu}^2-\tilde{\nu}_0^2+i\tilde{\nu}\gamma), \tag{2}$$

where μ is the dynamic dipole moment and the other quantities are defined as above, to arrive at a phenomenological line shape of Lorentzian form (valid for $\theta\leq85°$):

$$L_L(\tilde{\nu})\equiv\Delta R/R_0 = \frac{8e^2}{mc^2}\frac{\sin^2\theta}{\cos\theta}N_s\left[\frac{m}{m^*}\right]\left[\frac{e^*}{e}\right]^2\frac{\tilde{\nu}\gamma}{(\tilde{\nu}_0^2-\tilde{\nu}^2)^2+\gamma^2\tilde{\nu}^2}, \tag{3}$$

where e^*/e is identified as the normalized effective mi-

croscopic dynamic charge, m^*/m as the normalized effective mass of the oscillator, θ as the incident angle of the probe radiation with respect to the surface normal, and N_s as the coverage (atoms/cm^2). Other quantities are defined as above. In principle, a recorded spectral line shape that is strictly homogeneous would permit a precise evaluation of the parameters e^*/m^*, $\tilde{\nu}_0$, and γ.

A yet more general phenomenological line shape is the Fano form[35] that results from the interaction of a discrete level with a continuum. Langreth[21] generalized this idea to surfaces by showing that a line-shape asymmetry will necessarily result if the mode behavior is dominated by electronic damping of the oscillator. The total dynamic dipole μ associated with the adsorbate motion contains contributions from both the nuclei and the valence electrons. In general, the electronic response is out of phase with respect to the nuclear motion. When the adsorbate vibration is coupled to the substrate electrons, therefore, μ has both a real and imaginary part. The physical origin for the complex μ is this phase difference between electronic and nuclear response requiring an additional parameter $\tilde{\tau}$, which is termed the asymmetry parameter, to reproduce the line-shape asymmetry. The magnitude of $\tilde{\tau}$ represents the strength of the interaction. The form of the Fano line shape (valid for $\theta \leq 85°$) is

$$L_F(\tilde{\nu}) \equiv \Delta R/R_0 = \frac{8e^2}{mc^2}\frac{\sin^2\theta}{\cos\theta} N_s \left[\frac{m}{m^*}\right]\left[\frac{e^*}{e}\right]^2 \frac{(1-xy)^2}{(1+x)^2}, \quad (4)$$

where

$$x = \frac{\tilde{\nu}^2 - \tilde{\nu}_0^2}{\gamma\tilde{\nu}} \quad (5)$$

and

$$y = \tilde{\nu}\tilde{\tau}. \quad (6)$$

In the absence of strong coupling between the substrate and the oscillator valence electrons, corresponding to $\tilde{\tau}=0$, the Fano form reduces to the Lorentzian form.

Our procedure was first to isolate the infrared spectral region of interest, which would typically contain one to three vibrational features and a well-defined broadband electronic absorption. The vibrational features were then fit to each of the three phenomenological forms and the background was fitted to a power series. In the absence of a credible phenomenological form for background absorption, the power series was generally truncated at the linear or quadratic level. Changes in line-shape parameters due to background representation were included in the calculation of the error bars for the line-shape parameters. The line shapes chosen to represent each mode for H/Mo(100) and H/W(100) were based upon the reduced mean-square fitting errors of the least-squares fits of 100% H saturation data obtained at $T=100$ K.

To summarize, we analyzed the two vibrational features observed on W(100)-$p(1\times1)$H and Mo(100)-$p(1\times1)$H and described in Sec. IV B, as follows: The high-frequency H phonon mode for both the Mo(100)-$p(1\times1)$H and W(100)-$p(1\times1)$H was best represented by a Fano line shape; the low-frequency mode for Mo is of an irregular form that is equally well described by Lorentzian and Gaussian forms. We chose, somewhat arbitrarily, a Lorentzian parametrization for this mode to permit a better quantitative comparison to the W(100)-$p(1\times1)$H low-frequency mode, which is best fitted by a Lorentzian form. These respective forms were then utilized to fit the infrared reflectance spectra under a variety of adlayer composition and temperature-dependent conditions. The results of this procedure are presented in Sec. IV.

IV. RESULTS

A. Reference phases

Since the clean Mo(100) surface, characterized by (1×1) and $Ic(2\times2)$ LEED patterns above and below 200 K, respectively, cannot be used as a reference, the relevant H-stabilized phases used as references are described briefly. A full description and discussion of these phases is described elsewhere.[33] Recalling that phases with coverages less than 0.5 ML cannot be used because the system has not achieved sufficient thermal stability following the flash desorption, we concentrate on the features of the $[(z\times2)+c(2\times2)]$ and (2×1) phases as reference surfaces. Henceforth the $[(z\times2)+c(2\times2)]$ phase shall be abbreviated as the $(z\times2)$ phase.

This $(z\times2)$ phase, where z varies continuously from 4 to 3 upon increasing coverage, is useful to study the low-frequency mode (1016 cm^{-1}) of the (1×1) phase because its characteristic mode at 1240 cm^{-1}, as well as the weak contribution at 1270 cm^{-1} arising from the $c(2\times2)$ component, do not spectrally overlap with the modes of the saturation spectrum, particularly for the low-frequency mode. However, they lie rather close to the high-frequency mode (1302 cm^{-1}) of the (1×1) phase. It is also difficult to reproduce the same value of z each time, since the sticking coefficient is high within this phase. Furthermore, both the H vibrational contribution and the electronic contribution to the reflectivity spectrum vary as z ranges from 4 to 3. Thus, this $(z\times2)$ phase is in general an unsatisfactory standard reference and was utilized primarily as a double check of the line shape of the 1016-cm^{-1} mode.

In contrast, the (2×1) phase has a low H sticking coefficient and relatively small variations in electronic absorption from 1.2 to 1.4 ML. The vibrational spectrum is characterized by a relatively sharp (25 cm^{-1}) mode centered at 1116 cm^{-1}, which grows in intensity within the phase without shifting significantly. This (2×1) phase was therefore used extensively as a background reference to determine the line shapes for both the low- and high-frequency H modes on Mo(100). The accuracy of these line-shape determinations was then cross checked with the $(z\times2)$ reference phase. No significant line-shape errors were found to be introduced by our reference choice.

B. The pure (1×1) (saturation) phase

A summary of the spectroscopic constants determined for the H-saturated (1×1) phase on both Mo(100) and W(100) is presented in Table I(a). Figure 2(a) shows a

TABLE I. Spectroscopic constants (in cm^{-1} unless noted) determined for (a) the H-saturated surfaces of Mo(100) and W(100) and (b) the D-saturated W(100) surface.

Substrate	Mode	T (K)	$\tilde{\nu}_0$	FWHM	Asymmetry ($\tilde{\nu}_0\tilde{\tau}$)	e^*/e
			(a) Hydrogen			
Mo(100)	ν_1	100	1016(4)	65(5)		0.039(2)
	ν_1	245	1002(6)	72(10)		0.033(4)
	$2\nu_2$	100	1302(1)	12.2(5)	0.37(4)	0.024(1)
	$2\nu_2$	245	1300(1)	18(1)	0.40(4)	0.023(2)
W(100)	ν_1	100	1079(3)	47(5)		
	ν_1	300	1069(2)	103(8)		0.059(2)
	$2\nu_2$	100	1272(1)	18.5(10)	0.54(3)	
	$2\nu_2$	300	1269(1)	22(1)	0.53(3)	0.036(2)
			(b) Deuterium			
W(100)	ν_1	300	771	50		0.05
	$2\nu_2$	300	919	25	0.5	0.03

raw reflectance spectrum of the (1×1) phase referenced to a (2×1) background at $T=100$ K. To improve the signal-to-noise level and baseline stability, two Hg-Cd-Te detectors were used to cover the whole spectral region (broadband detector for the 800–1200-cm^{-1} region and narrowband detector for 1200–2200-cm^{-1} region) for the detailed line-shape measurements reported subsequently. For completeness, spectroscopic constants determined for the D-saturated W(100)-(1×1) surface are summarized in Table I(b). They differ slightly from those reported in Ref. 23, where only the $2\nu_2$ feature was fitted. However, it should be emphasized that error bars could not be determined due to the small number of runs. Therefore the constants of Table I(b) must be considered with caution.

The spectrum associated with the (1×1) $T=100$ K phase is characterized by a broad band centered at 1016 cm^{-1} [a full width at half maximum (FWHM) of 65 cm^{-1}] and a sharp, asymmetric feature at 1302 cm^{-1} (FWHM of 12.2 cm^{-1}). In analogy with previous ir measurements of H on W(100) (Ref. 36) and based on EELS studies of H on Mo(100),[12] the broad mode at 1016 cm^{-1} is assigned to the symmetric stretch mode (ν_1) of H at a twofold bridge position. Assuming that the saturation coverage is two H atoms per Mo surface atom, as for W(100),[33] this mode is identified as the in-phase symmetric stretch, the only *fundamental* mode that is dipole active. The feature at 1302 cm^{-1} is analogous to the 1269-cm^{-1} feature observed on W(100)-$p(1\times1)$H, which was previously assigned to the overtone of the wag mode, $2\nu_2$.[23,24] As will be further discussed in Sec. V A, the coverage at saturation is taken to be 2 ML and the 1302-cm^{-1} feature is also assigned to the overtone of the wag mode.

Beyond a justification of the mode assignment, the goal of the present work is to study the strength, frequency, line shape, and linewidth of these two modes as a function of isotopic and chemical substitution and as a function of temperature. Primary questions addressed include the following: why is the $2\nu_2$ mode observed with grazing-incidence ir reflection-absorption spectroscopy and not with EELS? What is the mechanism for enhancement of the overtone modes above the intensities estimated from purely vibrational (adiabatic) considerations? What is the nature of the substrate electronic structure that interacts with these modes? In particular, is the electronic density of states flat across the Fermi level, leading to a weak breakdown of adiabaticity, or strongly peaked, leading to a strong breakdown of adiabaticity?

C. Temperature dependence

The sample temperature fixes the highest-populated substrate phonon levels, as well as the density of electronic states occupied above the Fermi level. Consequently, hot band effects such as multiphonon decay processes, vibrational and electron-hole–pair dephasing, and electronic damping can be expected to exhibit a temperature dependence. The possible contributions from these processes to the hydrogen vibrational spectra can be assessed through the temperature dependence of the spectra.

The temperature onset for appreciable hydrogen desorption from the Mo(100) and W(100) surfaces under ultrahigh-vacuum conditions are 250 and 375 K,[37] respectively. To ensure a hydrogen-saturated surface, all measurements must therefore be made below these temperatures. In the case of H/Mo(100), spectroscopic measurements were performed at 4-cm^{-1} resolution with sample temperatures of 100 and 245 K. These data and the results of the linear least-squares-fitting procedure are presented in Fig. 3. The H/W(100) data were acquired at 8-cm^{-1} resolution at sample temperatures of 100 and 300 K. These data, and the corresponding 2-cm^{-1}–resolution measurements obtained at 300 K, are displayed together with the results of the fit in Fig. 4. Although this two-point temperature study is cursory at best, it does serve to constrain the level of detail of dynamical information that can be extracted from the line-shape analysis. The results of this temperature study

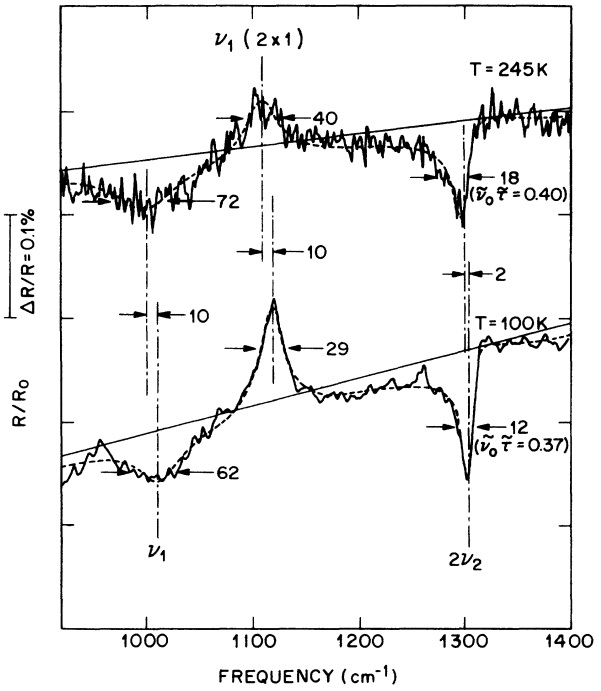

FIG. 3. Reflectance spectra of Mo(100)-$p(1\times1)$H, using the Mo(100)-(2×1)H surface as reference, at $T=245$ and 100 K. The dashed line is the result of a linear least-squares data fit, while the solid line denotes the linear portion of the fit, which represents electron absorption. Both spectra were obtained at 4-cm^{-1} resolution.

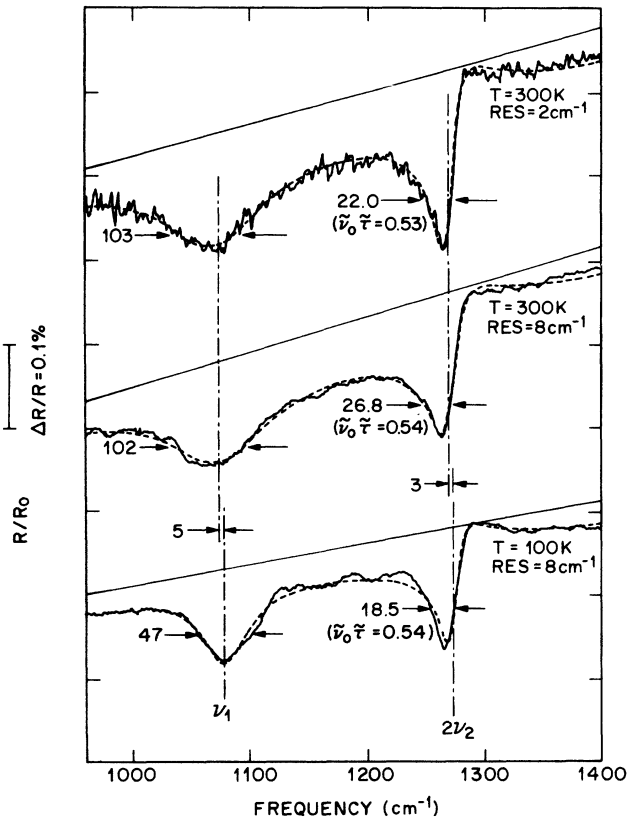

FIG. 4. Reflectance spectra of W(100)-$p(1\times1)$H, using the clean W(100) $Ic(2\times2)$ surface as reference. The results of a least-squares data fit are included as a dashed line, and the solid line represents the linear electronic contribution to the fit.

are listed in Table I(a). Note that only one 100-K run could be used for the fitting of H/W(100). Consequently, the error bars in Table I(a) are based solely on the least-squares fitting and are subject to larger systematic errors for the 100-K data.

A weak temperature dependence is observed for both the symmetric stretch mode ν_1 and the wag overtone $2\nu_2$ for Mo(100)-$p(1\times1)$H. This indicates that the linewidths cannot be uniquely associated with vibrational lifetimes. The sharp $2\nu_2$ mode is broadened by 50%, but is red-shifted by just 2 cm^{-1} upon increasing the temperature from 100 to 245 K. The asymmetry parameter, which monitors the strength of the interaction between the adsorbate vibration and the electronic excitations, remains, however, temperature insensitive. The ν_1 coordinate is also broadened (11%) and red-shifted (14 cm^{-1}) over the same temperature range. Similarly, the symmetric stretch of the (2×1) reference phase exhibits a thermal broadening (38%) and a red shift (10 cm^{-1}) upon increasing the temperature.

The spectroscopic behavior of W(100)-$p(1\times1)$H is virtually identical to that of H/Mo(100) with respect to $2\nu_2$, but differs with respect to ν_1. The resolution employed for the temperature-dependent studies (8 cm^{-1}) was sufficiently poor to modify artificially the line-shape parameters of the relatively sharp $2\nu_2$ mode from those precise values determined with higher resolution. However, the 8-cm^{-1} data can be consistently compared to other 8-cm^{-1} runs. We include in Table I the fitting results obtained at 2-cm^{-1} resolution to avail the most accurate line-shape parameters. Since only one low-temperature experiment was performed on W(100), the intensity decrease that corresponded to the increasing temperature for both modes has not been well characterized, but may result trivially from crystal misalignment. Consequently, this spectrum is only reliable to establish the temperature dependence of the mode wave numbers and widths.

The $2\nu_2$ mode is red-shifted (3 cm^{-1}) and broadened (20%), similar to Mo(100), upon increasing the temperature from 100 to 300 K. Furthermore, the asymmetry parameter, $\tilde{\nu}_0\tilde{\tau}=0.54$, is also insensitive to temperature, indicating that the asymmetry constant is indeed a measure of the interaction between the substrate electrons and the H motion. The ν_1 mode exhibits a relatively small red frequency shift, as on Mo(100), but is broadened by $>100\%$ upon increasing the temperature. At room temperature, therefore, the ν_1 linewidth on W(100) appears to be dominated by dephasing.

In summary, both ν_1 and $2\nu_2$ on Mo(100) and W(100) exhibit some thermal broadening. This broadening is substantial only for the ν_1 mode of W(100)-$p(1\times1)$H, however. The asymmetry parameters for $2\nu_2$ on both surfaces are completely temperature independent.

D. Hydrogen/Deuterium admixture experiments: Isotopic dependence

Monitoring the metal-hydrogen vibrational modes at constant coverage as a function of varying H/D concentration provides information concerning dynamical interactions, such as dipole-dipole or substrate-mediated interactions. It also helps to assess the role of long-range order, i.e., the possible added relevance of the $Q_{\parallel}=0$ modes, in determining mode intensities. Such isotopic mixing permits all chemical interactions to remain constant and the substrate atoms to remain in the same average positions since adsorbate-substrate phonon coupling is presumed negligible. As a result, the electronic structure is essentially unchanged. This is very different than the case of a chemically distinct co-adsorption (e.g., CO), for which the electronic structure can be altered significantly.

Figure 5 shows reflectance data characteristic at 40 at. % of hydrogen when small amounts of deuterium (0–40 at. %) are substituted at saturation coverage on Mo(100). The line shape of $2\nu_2$ is modified in addition to a weakening of both the ν_1 and $2\nu_2$ modes. Data over the 1900–2200-cm^{-1} region is also plotted to emphasize the point that negligible CO was co-adsorbed during these experiments. Indeed, as will be shown in Sec. IV F, very small amounts of CO can also alter the line shape substantially.

Figure 6 summarizes the fitting parameters as a function of H/D concentrations. For admixtures with less than 60% H, the Mo-H vibrational modes cannot be measured with sufficiently high signal-to-noise ratio. The intensities of the two modes are given in Fig. 6(a) by a plot of $(e^*/e)^2(N_s/N_s^0)$ versus N_s/N_s^0, where N_s is the H coverage and N_s^0 the total (saturation) coverage. In short, the abscissa in Figs. 6, 7, 11, and 12 is written N_s and expressed in percent. The unit slope of this plot indicates

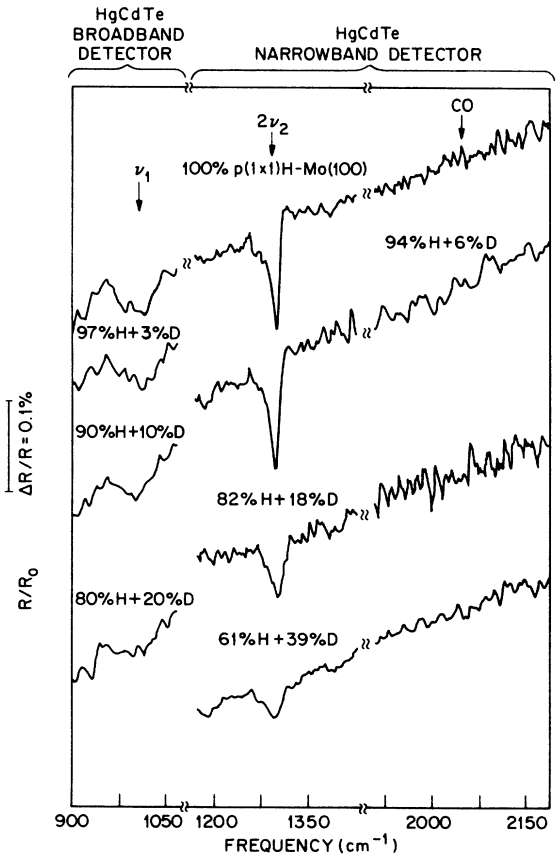

FIG. 5. H/D co-adsorption data at saturation coverage on Mo(100). Two detectors are used to cover the full spectral region with comparable signal-to-noise ratio. The Mo(100)-(2×1)H surface was used as reference and all data were obtained at 4-cm^{-1} resolution. The surface appears free of CO (<0.1% of a monolayer).

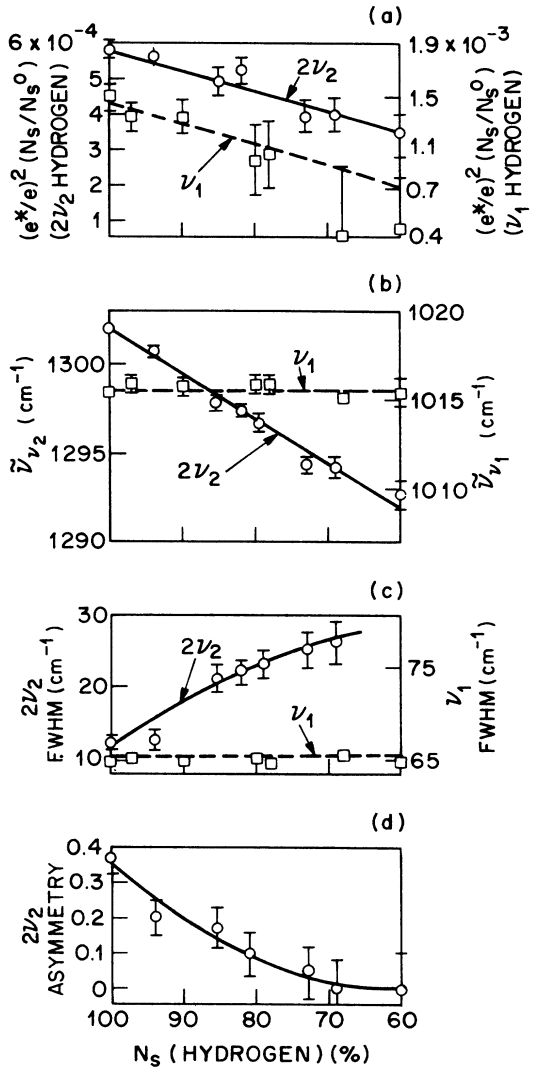

FIG. 6. Line-shape parameters for both the ν_1 and $2\nu_2$ H modes of Mo(100)-$p(1\times1)$H + D obtained from a least-squares fitting of the data for saturation coverage. The quantities $(e^*/e)^2(N_s/N_s^0)$ are obtained from the absolute-amplitude-fitting parameter of the line shapes. No additional normalization is necessary to relate measurement to measurement. The relative coverage N_s(H) was determined from multimass TDS. The solid line and dashed lines are intended solely to guide the eye through the $2\nu_2$ (circles) and ν_1 (squares) data points, respectively.

that at saturation coverage, the dipole strength per oscillator is independent of the isotopic purity of the hydrogen adlayer. This result confirms that the unusual intensity of the wag overtone is not due to a coherence effect associated with the $Q_{\parallel}=0$ phonon mode of the H layer.

No measurable shift is observed in the frequency of the ν_1 mode with D co-adsorption in Fig. 6(b), but a red shift in frequency (~ 10 cm^{-1}) of the $2\nu_2$ mode upon 30% D coadsorption is evident. Associated with this frequency shift are an increase in the FWHM from 12 to 28 cm^{-1}, observed in Fig. 6(c), and an apparent decrease in the asymmetry from $\tilde{\nu}_0\tilde{\tau}=0.4$ to 0.0 in Fig. 6(d).

A direct conclusion from Fig. 6, which shows that the intensities of both the H modes at saturation coverage are commensurate with the amount of hydrogen, is that the local-mode description is largely valid. The small frequency shift and broadening of the $2\nu_2$ mode can be attributed to dynamical coupling and mode dispersion. For the isotopically substituted system, $Q_{\parallel}$ is no longer a good quantum number to describe adlayer vibrations.[38,39] However, for low defect densities only a few values of $Q_{\parallel}$ are necessary to describe the vibrations observed. Thus, the recorded spectral profiles contain information concerning the mode dispersion, as well as the normal-mode spectrum of the inhomogeneous adlayer.

Some H/D co-adsorption data at saturation on W(100) has been reported previously.[23] Since temperature-programmed-desorption (TPD) calibration of the relative H/D coverage was not available for this earlier work, the relative H coverage was assumed to be linearly related to the integrated area of the ν_1 band (See Fig. 2 of Ref. 23). A multipeak least-squares fitting of the data, however, provides a more accurate method of delimiting the absorption by ν_1, $2\nu_2$, and the electronic background. Reexamining these data with improved procedures shows no significant departure from a constant ratio of the $2\nu_2/\nu_1$ mode strengths, validating the original results. As on Mo(100), the $2\nu_2$-mode intensity exhibits no enhancement for the pure hydrogen ($Q_{\parallel}\approx 0$) mode. Co-adsorbed D does, however, introduce a significant blue shift (~ 30 cm^{-1}) in the $2\nu_2$ mode, as shown in Fig. 7. The magnitude of this shift is comparable to that of $2\nu_2$ on Mo(100), but the direction, which is consistent with simple dipole-dipole interactions, is opposite. Note, however, that the shift is measured for less than 30% D on Mo(100) and only for more than 30% D on W(100).

The behavior of the ν_1 mode on W(100) is even more distinct, exhibiting a considerable narrowing ($\sim 50\%$) and a 10-cm^{-1} red frequency shift with increasing D relative concentration, as shown in Fig. 7. For the ν_1 stretch, therefore, dynamical interactions between H atoms, as evidenced by the line narrowing, appear stronger in W(100).

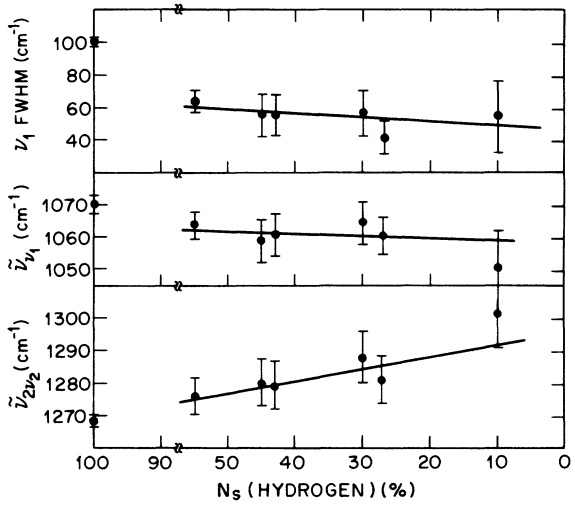

FIG. 7. H/D co-adsorption data for W(100)-$p(1\times1)$H + D, analyzed to determine the linewidths (top) and frequencies (center) of the ν_1(H) mode and frequencies of the $2\nu_2$(H) mode (below). All these quantities exhibit contrasting behavior as a function of N_s(H) to that on Mo(100). All parameters were determined through a least-squares data fit. The line drawn through the D-enriched region (see break) is intended as a guide to the eye.

E. Broadband reflectivities: Electronic absorption

In this section we compare the reflectivities of the different H phases on Mo(100) and W(100). We are thus able to identify surface-state absorption specific to the saturation (1×1) phases.

As noted by Anderson *et al.*,[40] Restorff and Drew[41] between 0.6 and 4.8 eV and by Riffe, Hanssen, and Sievers[42] at 0.125 eV, large changes in broadband surface absorption occur as a function of H coverage on W(100). These changes arise from the fact that the electronic absorption, which includes the surface-state and free-carrier absorption, is affected both by H bonding and W reconstruction at the surface. All these studies conclude that the clean W(100) surface displays surface-state band absorption. In particular, Riffe and co-workers[42] invoke the presence of a 0.4-eV intrinsic surface state on the clean W(100) to explain the changes in surface-electromagnetic-wave (SEW) absorption for $\Theta<0.42$ ML. They conclude that since the surface state is completely quenched at $\Theta=0.42$ ML [corresponding to the $Ic(2\times2)$ phase], any change in the electronic absorption above this coverage can only be due to a change in the electron-electron, electron-phonon, and electron-surface scattering, rather than in surface-state absorption. We will reexamine this conclusion shortly.

Such electronic absorption studies depend on the proper choice of a reference surface. In this regard, Riffe and co-workers[42] note that the $Ic(2\times2)$ phase has the lowest SEW absorption in the 1000-cm^{-1} region. We have also found that the $Ic(2\times2)$ phase has the highest reflectivity in the 800–3000-cm^{-1} range and we will therefore use this phase as a reference in the study of the electronic absorption of the (1×1) phase on W(100).

Although the number of phases on Mo(100) (see Fig. 1) is even larger than on W(100), similarities exist. In particular, a well-defined $c(2\times2)$ pattern is observed at $\Theta=0.5$ ML on Mo(100), as well as at $\Theta=0.33$ ML on W(100). On W(100), the $c(2\times2)$ phase continuously changes to an $Ic(2\times2)$ phase, while on Mo(100) it be-

comes a $(z\times2)$ phase, where z varies continuously between 4 and 3. The $(z\times2)$ and $Ic(2\times2)$ phases, however, are similar in that they are incommensurate with respect to the bulk lattice.[33] Significantly, we find that the reflectivity around 1000 cm^{-1} is also highest at the onset of the $(z\times2)$ phase on Mo(100), i.e., at $z=4$. We argue, therefore, that any intrinsic surface-state absorption has been quenched by the time the onset of the $(z\times2)$ appears and we use the $(z\times2)$ phase as a reference in the study of the electronic absorption of the (1×1) phase on Mo(100).

1. The clean W(100) surface

In order to ascertain the origin of the electronic absorption associated with the saturation phases, a thorough investigation of the reflectance of W(100) was performed over the whole coverage region $\Theta=0$–2 ML. In particular, the reflectance of the clean W(100) surface was expected to display a substantial contribution due to the 0.4-eV intrinsic surface state, thus giving representative reflectance magnitudes for such surface-state absorption. The data were recorded after the sample temperature was stabilized. For each run, the partial pressure of H (or D) was kept constant ($P=1\times10^{-8}$ torr, uncorrected) and the SIR spectra and LEED patterns recorded as a function of time (time resolution 10 s). In Fig. 8 the broadband spectrum associated with the clean W(100) surface, using the W(100)-$Ic(2\times2)$H phase as a reference, is plotted versus frequency. The clean W(100) surface clearly exhibits a substantial absorption with a maximum ($\Delta R/R\simeq0.7\%$) at 0.36 eV ($\sim$2900 cm^{-1}) indicated by the arrow labeled SS.

Since the $Ic(2\times2)$ phase is believed to be devoid of surface-state absorption, a very weak frequency dependence is expected in its broadband reflectivity. Therefore, the broad maximum observed in $(R_{\text{clean}})/\{R[Ic(2\times2)]\}$ is attributed to the absorption of the intrinsic surface state of the *clean* surface. As discussed in Sec. V E 3 a, this absorption is consistent with all of the previous studies of this surface state and with the symmetry of the excitations from this state.

2. The H-saturated W(100) and Mo(100) surfaces

The H-saturated surfaces of W(100) and Mo(100) were then investigated in a similar manner using the $Ic(2\times2)$ and $(z\times2)$ phases as references for W(100) and Mo(100), respectively. The reflectance ratios of $(1\times1)/[Ic(2\times2)]$ for H/W and D/W, and $(1\times1)/(z\times2)$ for H/Mo are plotted in Fig. 9. Both (1×1) phases have substantial electronic absorption below 3000 cm^{-1} with respect to the reference phases (hatched area). The error bars indicate our estimate of the systematic errors associated with the source stability and the sample temperature and position stability during the whole run. The W data are more accurate than the Mo data because low-resolution (16-cm^{-1}) runs were taken every 10 s as the surface was continuously exposed to H or D until saturation ($\sim$4.5 L). [1 langmuir (L)$\equiv10^{-6}$ Torr s]. The Mo data acquisition used longer scan times, making it difficult to return reproducibly to the same point of the Θ-T phase diagram. Details of the measurement accuracy are given in the Appendix. Two important observations are made: (1) the absorption increases with decreasing energy for the (1×1) phases on both W(100) and Mo(100), and (2) the

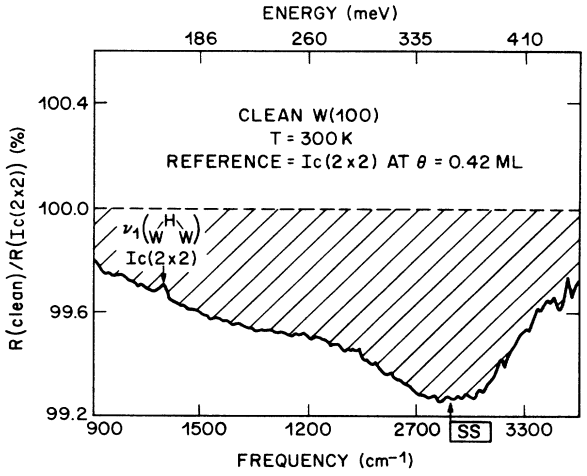

FIG. 8. Broadband reflectance absorption spectrum associated with the clean W(100) surface. The data were recorded at 300 K, using the H-induced $Ic(2\times2)$ phase as a reference ($\Theta=0.42$ ML). The resolution is 16 cm^{-1}. The broad band peaking around 2900 cm^{-1} at the point labeled SS corresponds to an absorption of the clean W(100) surface. The sharper, inverted peak at 1290 cm^{-1} corresponds to the ν_1 vibrational absorption of the $Ic(2\times2)$ reference phase. For details on the measurement accuracy, see the Appendix.

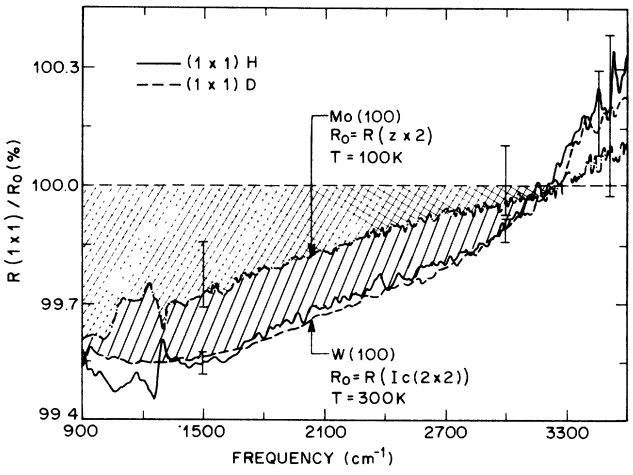

FIG. 9. Broadband reflectance spectra of Mo(100)-$p(1\times1)$H (dotted-dashed-line), W(100)-$p(1\times1)$H (solid line), and W(100)-$p(1\times1)$D (dashed line), using the highest-reflectivity, lower-coverage phases, Mo(100)-$(z\times2)$H and W(100)-$Ic(2\times2)$H, as references. The reduction in reflectance for both Mo(100) (cross-hatched area) and W(100) (hatched and cross-hatched area) is indicative of additional electronic absorption by the saturation phases, i.e., surface-state absorption in the low-frequency region, centered $\sim$0.12 eV below E_F. For details on the measurement accuracy, see the Appendix.

relative absorption of W(100)-(1×1)H is larger than that of Mo(100)-(1×1)H.

In the case of Mo(100), systematic reflectance measurements for all the ordered phases above $\Theta=0.5$ ML clearly showed that the low-frequency absorption, observed in the spectrum of the (1×1) phase, appears *after* the 2×1 phase vanishes. This result demonstrates that only the (1×1) surface phase of H/Mo(100) has additional electronic absorption at low frequencies, similar to that of H/W(100). Such an increase in absorption at saturation coverage is not observed for other adsorbates such as O, N, and CO.[43]

F. H/CO co-adsorption

A comparison of the broadband (electronic) and vibrational absorption intensities documented in Figs. 8 and 9 demonstrates their comparable magnitude for our given grazing incidence and *p*-polarized radiation conditions. The broadband reflectivity studies further demonstrate the presence of the 0.36-eV intrinsic surface state on the clean W(100) surface, as previously invoked by Riffe and co-workers,[42] and significant electronic absorption specific to the saturation phases, i.e., $p(1\times1)$ surface states. The extent to which the vibrational modes of the H adlayer are coupled to the near-surface-substrate-electronic structure was investigated through H/CO saturation co-adsorption measurements on Mo(100).

CO is known to modify the electronic structure near the surface by donating σ-electron density to the metal substrate and drawing charge density from the metal *d* bands into its empty low-lying $2\pi^*$ orbitals.[44] At 100 K CO is immobile on the Mo(100) surface, preventing island formation. The near-surface-electronic structure of a "H-saturated" Mo(100) surface can thus be altered by first preparing the Mo(100)-(2×1)H reference phase by hydrogen dosing, then exposing with small quantities of CO, the electronic modifying agent, and subsequently saturating the surface with hydrogen. The continued observation of both the ν_1 and $2\nu_2$ modes characteristic of the (1×1) H phase, in addition to the high-frequency (1900–2200 cm^{-1}) bands characteristic of the CO stretch, indicate that the local bonding configuration of the hydrogen adsorbate has not been altered by the co-adsorbed CO.

The absolute amount of hydrogen present on the surface was determined by integration of the hydrogen thermal desorption peak for each spectroscopic measurement and comparing this integrated H area to that of a pure Mo(100)-(1×1)H surface. CO desorbs from the surface at a much higher temperature ($T>800$ K) (Ref. 45) than H and was not observed under the conditions of our thermal desorption measurements. However, the relative amount of CO present on the surface, deduced from the H thermal desorption measurements, was in quantitative agreement with the relative CO exposure conditions.

The H $2\nu_2$ band and the CO stretching bands observed with 0–15 % of the H sites blocked by CO coadsorption are presented in Fig. 10. These observations were quantified through the least-squares fitting of the H $2\nu_2$ mode to the Fano form and of the CO bands to three Lorentzian forms with the broadband background in both cases represented linearly. Over the range of conditions investigated, we found that three Lorentzians were necessary to reproduce the complex CO band.

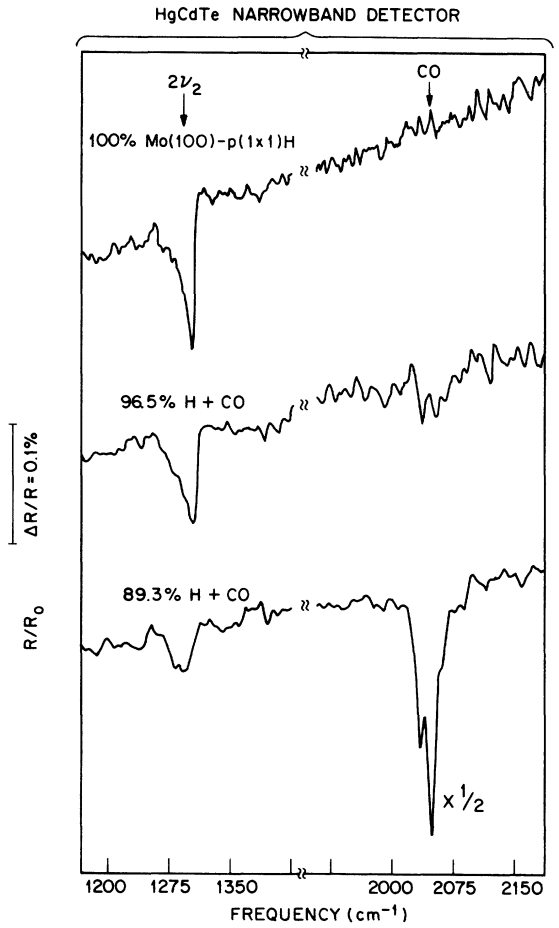

FIG. 10. H/CO co-adsorption data obtained at $T=100$ K on Mo(100). The relative coverage N_s(H) was determined by integration of the H_2 TDS signal.

The most significant result of these measurements is the relative intensities of the H $2\nu_2$ band and the CO stretching band as a function of relative hydrogen coverage, N_s(H). Unlike the case of H/D co-adsorption, the value of e^*/e for H $2\nu_2$ is not a constant independent of N_s(H), as evidenced in Fig. 11 by a deviation of the plot of $(e^*/e)[N_s(\mathrm{H})/N_s^0]$ versus N_s(H) from a line with unit slope. The intensity of the CO band, monitored as the sum of the intensities of the three Lorentzians needed to fit the band, does retain a constant value of e^*/e. These results indicate that the effective dipole of the H wag overtone ($2\nu_2$) is reduced by the presence of the co-adsorbed CO.

The line-shape parameters for the $2\nu_2$ mode are all affected by the co-adsorbed CO, as seen in Fig. 12. A slightly larger red frequency shift of the $2\nu_2$ mean (1302–1292 cm^{-1}) is evident over the 100–86.7 at. % range of N_s(H) studied than for the comparable N_s(H) range reported for H/D co-adsorption. The $2\nu_2$ width

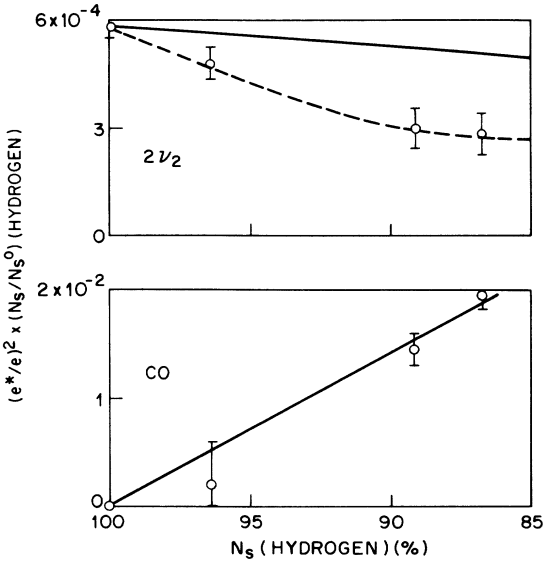

FIG. 11. Relative intensities of the Mo-H-Mo $2\nu_2$ mode (top) and CO stretch (bottom) as a function of N_s(H) on Mo(100). The solid lines project those intensities expected for constant values of the dynamic dipole moment $(e^*/e)^2$. In the case of $2\nu_2$, the dashed line indicates a departure from a constant $(e^*/e)^2(2\nu_2)$ value for increasing CO coverage.

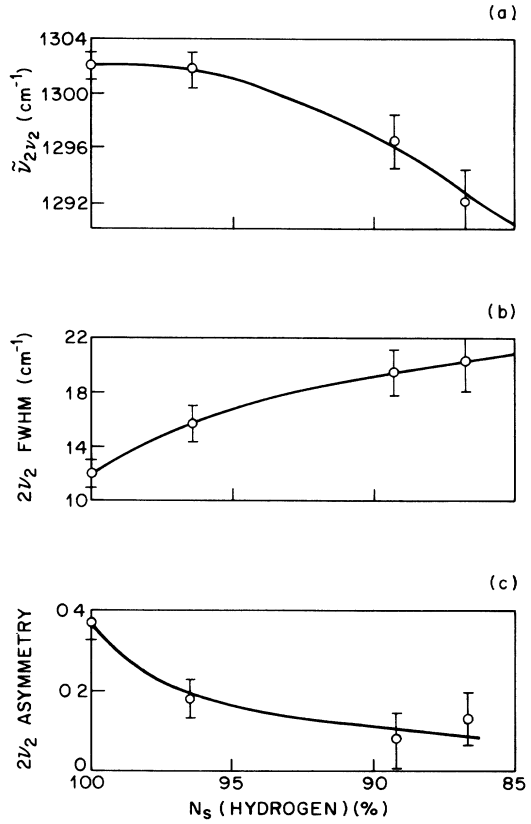

FIG. 12. Line-shape parameters determined for the Mo-H-Mo (or Mo_2H) $2\nu_2$ mode for the H/CO co-adsorption data. The lines are intended solely to guide the eye.

and asymmetry parameters, however, follow a comparable dependence on N_s(H) in the presence of CO as in the presence of substituent D. Furthermore, the profile of the CO band was virtually constant over the range of studies. The three Lorentzian features for all N_s(H) are described by mean frequencies of 2035(2), 2049(2), and 2062(2) cm^{-1} with respective FWHM values of 10(1), 12(2), and 10(2) cm^{-1}. The insensitivity of the CO band profile to the amount of CO present on the surface is taken as a confirmation that islanding is not occurring on the surface at 100 K.

In short, co-adsorbed CO attenuates the dynamical dipole of the $2\nu_2$ mode, but does not otherwise appreciably alter the line-shape parameters in a manner different to D. An interpretation of this result based on electronic and harmonic considerations is presented in Sec. V F.

V. DISCUSSION

A. Mode assignment

In order to discuss the spectroscopy and dynamics of $p(1\times1)$ H on Mo(100) and W(100), the spectral assignment must first be established. Our assignment of the vibrational features observed on the Mo(100)-$p(1\times1)$H surface is based largely upon analogy to the semblable W(100)-$p(1\times1)$H surface. The vibrational assignment of the latter system was definitely constructed from an array of experimental evidence (EELS, ir, ion channeling, quantitative TDS), which is not so extensively available for H/Mo(100).

To briefly review the H/W(100) mode assignment, the unit cell at saturation coverage is of C_{4v} symmetry and possesses two H atoms per W atom. Of the three possible high-symmetry H sites—a top, twofold bridge, and fourfold hollow—only the twofold bridge location would give rise to a symmetric stretch that occurs in the 1000–1300-cm^{-1} region. The twofold bridge site is also characterized by an infrared-inactive wag mode, ν_2, which has been identified by off specular EELS at $\nu_2=645$ cm^{-1}.[26] Although the fundamental ν_2 is not infrared active, the first overtone, $2\nu_2$, has some dipole character[23,24,46] and falls within the region of investigation. The derivative-like feature at 1269 cm^{-1} for H/W(100) was consequently assigned to $2\nu_2$, requiring an anharmonicity of just 1.5% to relate this feature to the fundamental. Alternatively, the 1269-cm^{-1} mode might be assigned to a phonon sideband of ν_1. Since bulk-phonon frequencies as high as 225 cm^{-1} have been reported with a maximum in all the bulk-phonon density of states of 210 cm^{-1},[47] this assignment would be energetically possible. However, since the two features exhibit decidely different shapes, the $2\nu_2$ assignment is preferred.

In the case of H/Mo(100), we begin by assuming a saturation coverage of two H atoms per Mo atom. This assumption is consistent with the series of H-induced LEED patterns that this system undergoes, which maintain some congruity to the H/W(100) system. The C_{4v} symmetry of the H-saturated surface is the same as for H/W(100), placing the same frequency restrictions for hydrogen modes associated with particular high-symmetry sites. We are led, therefore, to assign $\Theta=2$

ML hydrogen to a twofold bridge position on Mo(100). This bridge site was proposed from the recent EELS study as well, on the basis of similar arguments and the linear sensitivity of the ν_1 intensity to co-adsorbed sulfur.[12] The derivative-like absorption that we observe at 1302 cm^{-1}, which was absent from the EELS spectra, is analogous to the 1269-cm^{-1} feature on W(100). This absorption is assigned accordingly to the $2\nu_2$ mode for H on Mo(100).

For completeness, we also looked for evidence of the $2\nu_3$ transition, the first overtone of the asymmetric stretch mode, which is also dipole allowed. The $2\nu_3$ feature would occur at 2540 cm^{-1} for W(100)-$p(1\times1)$H, neglecting anharmonicity. We observe no vibrational absorption above the noise level, $\Delta R/R_0 = 2.5\times10^{-4}$, in this frequency region, thus setting an upper limit on the dynamic effective charge, $(e^*/e)^2(2\nu_3)/(e^*/e)^2(2\nu_2) < 0.1$, assuming comparable linewidths for $2\nu_2$ and $2\nu_3$.

B. Line shapes and $2\nu_2$ intensities: General considerations

The derivative-like shape and unexpected intensity of the $2\nu_2$ feature and the large width of the ν_1 band on both substrates are the main puzzles we address beyond the mode identification. We attempt to identify the dynamics responsible for the infrared characteristics of $2\nu_2$ and distinguish between homogeneous and inhomogeneous contributions to the line shapes of both ν_1 and $2\nu_2$. In order to sort out these effects, a brief summary of the possible broadening and/or shape-defining processes and their dependence on our experimental "variables"—substrate, temperature, surface inhomogeneities (defect, impurities, etc.), D co-adsorption, and CO co-adsorption—is presented. We argue that the $2\nu_2$-mode intensity and shape is largely nonadiabatic in origin, resulting from the coupling between surface-electronic states of the $p(1\times1)$ phase and $2\nu_2$ vibration. Broadening due to dephasing is evident for both ν_1 and $2\nu_2$, apparently dominating the ν_1 line shape on W(100), and substrate phonons are considered the most likely dephasing channel.

A variety of mechanisms can affect the shapes and widths of infrared vibrational absorption. These mechanisms can be categorized by dissipative damping (T_1), dephasing (T_2), and inhomogeneous broadening processes.[19] Identifying the relative importance of these mechanisms is complicated by the fact that all can exhibit temperature and isotopic dependence. Vibrational lifetime processes include decay via substrate phonon generation, via substrate-electronic excitation (electron-hole–pair generation), and via excitation of other adlayer vibrations. In addition to affecting line shapes, substrate phonons[48] and electronic states[21] provide continuum decay channels and can enhance the strength of a vibrational feature beyond the adiabatic intensity. Such enhancement arises from the fact that the sharp vibrational mode modulates the absorption by the continuum, which can, in fact, be much larger than the pure vibrational absorption, particularly in the case of a strong breakdown of adiabaticity. The interference between the discrete vibrational level and the continuum is manifested as an asymmetric line shape. As shown by Langreth, this asymmetry is a direct result of the phase difference in the response of the continuum and the discrete vibrational mode to the electromagnetic excitation. Both intensity borrowing and line-shape asymmetry are evident in the phenomenological line-shape function derived by Langreth and given in Eq. (4).

Among several first-principle calculations,[49–51] the recent linear-augmented-plane wave (LAPW) calculations of Biswas and Hamann[50] for W(100)-$p(1\times1)$H make it possible to estimate the adiabatic dynamic dipole moment associated with all the vibrational modes at saturation. The calculated effective charge and wave number of the ν_1 mode are $e^*/e = 0.03$ and $\tilde{\nu} = 1137$ cm^{-1}. With regard to $2\nu_2$, however, the calculation discerned no change in the work function (ϕ) as H is translated along the wag motion, thus establishing a strict upper limit $d\phi/dz < 0.025$ a.u. An estimate of the adiabatic value of e^*/e for $2\nu_2$ may be obtained by utilizing the relationship

$$\frac{\partial\mu}{\partial z} = \frac{1}{4\pi n}\frac{d\phi}{dz}\ , \tag{7}$$

where $\partial\mu/\partial z$ represents the dynamic dipole moment per atom, n represents the number of atoms moved per unit area, and $d\phi/dz$ is the derivative of the work function with respect to the surface normal. The form for the cross section for dipole excitation is

$$|\langle 2\nu_2 | \mu_{\rm op} | 0\rangle|^2\ . \tag{8}$$

Using the work-function limit and approximating the vibrational wave functions as harmonic oscillators, we calculate $(e^*/e)(2\nu_2) < 0.014$. A more precise calculation may, in fact, set a much lower limit. However, even this upper limit for $(e^*/e)(2\nu_2)$ falls short of the measured value for W(100)-$p(1\times1)$H, $(e^*/e)(2\nu_2) = 0.036$, indicating that a purely adiabatic process cannot account for the observed $2\nu_2$ line strength.

The asymmetry of the $2\nu_2$ mode on both W(100) and Mo(100) is a strong indication that the $2\nu_2$ level is interacting with a continuum. We first consider the substrate phonon continuum as the interference channel. This channel would require the interference between the discrete hydrogen vibration and multiphonon substrate continuum levels (number of quanta >4), since substrate phonons are considerably softer than hydrogen vibrations. Direct infrared excitation of such multiphonon substrate levels is very inefficient and is unlikely to account for the intensity enhancement of the $2\nu_2$ modes. In contrast, the density of electronic states in the vicinity of the Fermi edge for metals is relatively high and only single quantum excitations are necessary to produce electron-hole pairs isoenergetic with the wag overtone. In particular, the electronic-structure calculations of Richter and Wilkins[49] explicitly show the presence of states with d_{xy} symmetry (e.g., at $\bar{\Gamma}$ and $\bar{X}$), located in the immediate vicinity of E_F ($\lesssim 0.1$ eV). Intraband transitions provide, therefore, the continuum absorption with the proper symmetry to couple to $2\nu_2$.[23] We further demonstrate in Sec. V E that, in contrast to EELS, grazing-incidence p-polarized radiation can effectively ex-

cite substrate-electronic transitions of parallel dipole character, $\epsilon_{\parallel}$.

Comparison of the results presented in Table I show that the width γ, the asymmetry $\tilde{\nu}_0\tilde{\tau}$, and the effective charge (e^*/e) of the $2\nu_2$ feature display *no* measurable isotopic dependence (within experimental accuracy). This behavior is consistent with recent predictions for the case of a *strong* breakdown of adiabaticity[52] that derive *no* isotopic dependence for $\tilde{\nu}_0\tilde{\tau}$, and only a weak dependence for $\tilde{\gamma}(M^{-1/2})$ and $e^*(M^{-1/4})$. In contrast, predictions for the case of *weak* breakdown of adiabaticity give a stronger isotopic dependence for $\tilde{\nu}_0\tilde{\tau}(M^{-1/2})$ and $\gamma(M^{-1})$ than measured experimentally.

We wish to emphasize that this substrate-electron–hydrogen-phonon interference channel is a direct result of the vibrational-mode dynamics and is distinct from "dispersion asymmetry" observed in thick layers.[53] Indeed, vibrational modes of such thick layers can exhibit dispersion asymmetry due to a large dispersion in the index of refraction of the thick layer itself. However, such a dispersion asymmetry is present in all the vibrational modes of the layer. Conclusively, all the vibrational modes for H/W(100) and H/Mo(100) do not exhibit an asymmetry. The very small charge transfer measured for the W-H and Mo-H layers and corresponding weak dynamic dipole moments, furthermore, indicate that the dielectric function associated with this layer has a very small imaginary part and therefore negligible dispersion. Dispersion asymmetry can thus be ruled out and the $2\nu_2$ line shapes and intensities attributed to nonadiabatic coupling to substrate-continuum-electronic states.

We now return to other processes that can affect the observed line shapes for both ν_1 and $2\nu_2$. Unfortunately, inhomogeneous broadening can never be completely eliminated from line-shape considerations.[20] In the present study of Mo(100) and W(100), however, the data were accumulated and reproduced over periods of several months. Thus it could be established that any defect- or contamination-induced effects present in the reported data for both modes are significantly smaller than those effects that are introduced through variations of temperature or adlayer composition. The ν_1 linewidths are very broad for the $p(1\times1)$ phase on both surfaces, but do not result primarily from surface inhomogeneities. For H/D co-adsorption at saturation coverage on W(100), for instance, we note that a substantial narrowing from 102 to 65 cm^{-1} is observed for ν_1 upon introducing 45% D. Dynamical interactions are thus observed to dominate the ν_1 width on W(100) at saturation coverage. Significantly, the ν_1 linewidths corresponding to lowest-coverage hydrogen phases at $T=100$ K on Mo(100), e.g., $\gamma(2\times1)=25$ cm^{-1}, $\gamma(c(2\times2))=40$ cm^{-1}, are in many cases considerably narrower than for the more uniform $p(1\times1)$ saturation phase. Factors other than inhomogeneous broadening dominate the ν_1 line shape at saturation coverage.

It is perhaps most difficult to assess the contributions from T_2-type processes to the spectral profiles. These T_2 processes encompass quasielastic-scattering events between the adlayer vibrations and substrate defects, phonons, *e-h* pairs, and exchange coupling. Defect scattering, like inhomogeneous broadening, should have but a weak temperature and adlayer composition dependence. The phonon-dephasing and exchange-coupling channels should produce an exponential temperature dependence in the low-temperature limit, and an appreciable adlayer composition dependence, with respect to observed linewidths. This temperature dependence can be related to an effective frequency for the dephasing channel.[54] Electron-hole–pair dephasing could also produce a strong ($\sim T^3$) temperature-dependent contribution.[55] We examine both ν_1 and $2\nu_2$ linewidths for evidence of T_2-type processes. The Fano shape of $2\nu_2$ and its unexpected intensity beyond adiabatic considerations cannot, however, result from T_2-type processes.

C. Temperature dependence

We now discuss the experimental evidence in the framework of the decay models, beginning with a comparison of the two substrates for isotopically pure adlayers. The 100-K data for ν_1 for Mo(100) and W(100) indicate a comparable, but broad peak, which is red-shifted upon increasing temperature. In the case of W(100), where the absorption lines are more intense, the ν_1 width is found to double upon increasing the temperature to 300 K. The broadening is not as dramatic for Mo(100), but larger error bars due to lower signal levels cannot rule out broadening. In fact, causality[19] suggests that the red shift (19 cm^{-1}) of the ν_1 peak, which is evaluated more accurately than the width, must be accompanied by a corresponding change in width. These changing linewidths can be related to changes in Boltzmann population of low-frequency dephasing channels characterized by an effective frequency ν_{eff} [$\nu_{\text{eff}}\leq 510$ cm^{-1} for W(100) and $\nu_{\text{eff}}\lesssim 70$ cm^{-1} for Mo(100)]. In the case of W(100), H/D co-adsorption results indicated a significant dynamic coupling, which we do not consider in the computation of ν_{eff}. Thus, the computation assumes all broadening is due to dephasing, and overestimates ν_{eff}. Among the possible dephasing channels in this low-frequency region are substrate phonons and electron-hole pairs. Recalling that hydrogen ν_1 modes exhibit a range of frequencies (1000–1300 cm^{-1}) for the lower-coverage phases, corresponding to changes in the Mo-Mo and W-W dimer length, we find it consistent that substrate phonons should introduce substantial broadening of the $p(1\times1)$ ν_1 vibrations through dephasing.

Comparable thermal broadening is observed for $2\nu_2$ on both Mo(100) and W(100), indicating that a similar low-frequency dephasing process is active for these modes [$\nu_{\text{eff}}\leq 110$ cm^{-1} for W(100) and 285 cm^{-1} for Mo(100)]. However, the line-shape asymmetries of $2\nu_2$ modes, arising from nonadiabatic interactions, do not exhibit a temperature dependence. The thermal broadening of $2\nu_2$ indicates that dephasing can partly contribute to the width of the feature, but the fixed asymmetry suggests that the dynamics are dominated by electronic interactions. Consequently, the linewidths extracted from the fits at the lowest temperatures (~ 100 K) can be used to set a lower

bound for the vibrational lifetimes. On W(100), $\gamma = 18.5$ cm^{-1} gives $T_1 \gtrsim 0.9$ ps, and on Mo(100), $\gamma = 12.2$ cm^{-1} gives $T_1 \gtrsim 0.6$ ps.

D. Isotopic dependence

The H/D co-adsorption data at saturation coverage gauges the dependence of ν_1 on $Q_{\parallel}$, dipole coupling and surface homogeneity, without significantly modifying the electronic properties. The H ν_1 mode on Mo(100) appears insensitive to adlayer composition for the H/D layer, retaining a fixed mean of 1016 cm^{-1}, width of 65 cm^{-1}, and an intensity linearly dependent on N_s(H) for up to 40% co-adsorbed D. In the case of W(100), however, some shifting upon co-adsorption of D is manifested, together with significant peak narrowing (100 to 60 cm^{-1} for 0–40 % D). Over the 40–90 % D range, however, the ν_1 parameters remain fairly constant for W(100). We point out, however, that the H/D co-adsorption data were obtained at 100 K for Mo(100) and at 300 K for W(100), introducing some ambiguity in contrasting their behavior.

It is clear that the H compositional purity on Mo(100) is not a dominant factor in the large ν_1 width, diminishing the importance of vibrational decay via other H modes and dipole coupling as a source of its large linewidth. In the case of W(100) at 300 K, we expect dipole coupling to be somewhat stronger than on Mo(100), corresponding to the larger dynamic dipole moment. The large change in ν_1 parameters upon co-adsorption of D may be attributed to reduced dynamic coupling. Since dephasing is also evident at 300 K, the line narrowing upon D co-adsorption may indicate that dephasing is facilitated for the isotopically pure H layer on W(100). At $T = 100$ K on Mo(100) the dephasing is already substantially reduced, and line narrowing due to D co-adsorption would be less evident.

Another possibility is that the ν_1 width is due to an electronic decay via e-h–pair generation, and that deuterium co-adsorption shifts the zero-point motion of the adlayer phonon modes (20 cm^{-1}) to couple differently with the substrate-electronic structure. This latter process would, however, not exhibit a strong temperature dependence, nor would a small zero-point shift change damping characteristics so markedly. Consequently, we favor a T_2 dephasing process through substrate phonons to account for the temperature-dependent width of the ν_1 feature on both Mo(100) and W(100). Apparently a much lower temperature than $T = 100$ K is necessary to freeze out substrate phonons and yield a natural linewidth for the ν_1 mode. The large linewidths observed for symmetric stretching modes of H on a number of substrates,[56,57] suggest that this process may be a general feature of hydrogen phonons on metals.

The $2\nu_2$ band appears to be more sensitive to isotopic composition than ν_1 because it is sharper and better defined. There is an appreciable (14-cm^{-1}) shift in the $2\nu_2$(H) wave number on Mo(100) with associated broadening for the co-adsorbed 0–40 % D concentration range, which is significant compared to the 12-cm^{-1} linewidth of the isotopically pure H layer. On W(100), there is also a notable ($\sim$30-cm^{-1}) overall shift in the $2\nu_2$(H) wave number for the co-adsorbed 0–90 % D concentration.

These line-shape modifications can be accounted for by adlayer isotopic inhomogeneity as long as some dispersion characterizes the mode of the isotopically pure layer.[38] However, if dispersion broadening were the sole mechanism, a different sign in the dispersion of the ν_2 mode on Mo(100) would be required from that of ν_2 on W(100). It is likely therefore that the coupling to the continuum is also frequency dependent. Since the value of $(e^*/e)(2\nu_2)$ remains constant as a function of N_s, the relative H concentration, the coupling of the $2\nu_2$ mode and continuum remains constant and the shift and broadening is due to inhomogeneities (dispersion broadening and/or frequency-dependent coupling).

E. Surface-electronic absorption

To quantify the broadband reflectance measurements described in Sec. IV E and to investigate the physical origin of the electronic continuum, the expressions derived in Ref. 1 for the electronic absorption taking place *within* the substrate are first presented. The contribution of electron-scattering mechanisms to the observed absorption is then considered and mostly discounted. Instead, the contribution of surface-state absorption, both for the clean W(100) surface and the H-saturated W(100) and Mo(100) surfaces, is shown to account for the data.

1. General

The reflectivity of a metal, characterized by a complex anisotropic dielectric function $\tilde{\epsilon}_i^m$ (where $i = x,y,z$), for an electromagnetic radiation incident at an angle θ is approximately

$$R_{p\ \mathrm{pol}} \approx 1 - 4\,\mathrm{Re}(\tilde{\epsilon}_x^m)^{-1/2}/\cos\theta\ , \tag{9}$$

and

$$R_{s\ \mathrm{pol}} \approx 1 - 4\,\mathrm{Re}(\tilde{\epsilon}_y^m)^{-1/2}\cos\theta\ , \tag{10}$$

where the approximations $|\tilde{\epsilon}_i^m| \gg 1$ and $\cos^2\theta \gg |\tilde{\epsilon}_i^m|^{-1}$ have been made, as they are appropriate for radiation incident at $\theta = 85°$ on W and Mo in the 700–2000-cm^{-1} region. The subscripts correspond to the axes defined with $\hat{z}$ normal to the surface, $\hat{x}$ tangential and in the incidence plane, and $\hat{y}$ tangential and normal to the incidence plane.

We now assume that there is an additional electronic absorption localized at the surface and model it with a layer of thickness d_i and dielectric function $\tilde{\epsilon}_i$ ($i = x,y,z$), which is large (i.e., of the same order as $\tilde{\epsilon}_i^m$).[1] The *surface* absorption measured in a reflection absorption experiment is

$$\left.\frac{\Delta R}{R_0}\right|_{p\ \mathrm{pol}} \equiv \left.\frac{R_0 - R}{R_0}\right|_{p\ \mathrm{pol}} \approx 8\pi\tilde{\nu} d_x \frac{1}{\cos\theta}\,\mathrm{Im}\left[\frac{-\tilde{\epsilon}_x}{\tilde{\epsilon}_x^m}\right] \tag{11}$$

and

$$\left.\frac{\Delta R}{R_0}\right|_{s\ \mathrm{pol}} \equiv \left.\frac{R_0-R}{R_0}\right|_{s\ \mathrm{pol}} \approx 8\pi\tilde{\nu}d_y\cos\theta\ \mathrm{Im}\left[\frac{-\tilde{\epsilon}_y}{\tilde{\epsilon}_y^m}\right] . \tag{12}$$

We note that all the terms involving the normal component of the dielectric functions, $\tilde{\epsilon}_z^m$ in Eqs. (9) and (10) and $\tilde{\epsilon}_z$ in Eqs. (11) and (12), are very small compared to the terms involving the tangential components and can be neglected. This selectivity arises from the strong refraction of the radiation within the substrate, resulting in substantial sensitivity to the tangential components of $\tilde{\epsilon}$ only. Furthermore, a comparison of the geometrical factor in Eqs. (9)–(12), $1/\cos\theta$ and $\cos\theta$, indicates very different magnitudes for $\Delta R/R_0|_{p\ \mathrm{pol}}$ and $\Delta R/R_0|_{s\ \mathrm{pol}}$ at $\theta=85°$: the p-polarized radiation electronic absorption is more than 100 times stronger than the s-polarized radiation electronic absorption. This results from the large penetration of both the tangential and normal components of the incident electron field into the metal as the pseudo-Brewster angle is approached, i.e., for p polarization only.

If we impose a Drude description of the metals, characterized by a plasma frequency ω_p and an electron relaxation time τ, then we find that both W and Mo for $T\lesssim 300$ K are in the extreme relaxation regime $[(\omega\tau)^2\gg 1]$ with approximate expressions for the dielectric function, $\tilde{\epsilon}=\epsilon'+i\epsilon''$:

$$\epsilon'\approx -(\omega_p/\omega)^2 \quad \text{and} \quad \epsilon''\approx(\omega_p/\omega)^2(1/\omega\tau) . \tag{13}$$

The possible contributions to the surface-electronic absorption fall into two categories. The first class of mechanism affects the scattering rate, τ^{-1}, and encompasses (1) the electron-electron interactions, (2) the electron-phonon interactions, and (3) the electron collisions with the surface.[42] The second class involves electronic transitions such as in surface-state absorption and can be modeled within the Drude picture by altering both ω_p and τ for a thin surface layer.

From electron-scattering mechanisms (only τ is modified to τ_s), Eqs. (11) and (12) give, in the extreme relaxation limit $[(\omega\tau)^2\gg 1]$,

$$\left.\frac{\Delta R}{R_0}\right|_{p\ \mathrm{pol}} = 4(d_x/c)(1/\cos\theta)(1/\tau_s-1/\tau) , \tag{14}$$

$$\left.\frac{\Delta R}{R_0}\right|_{s\ \mathrm{pol}} = 4(d_y/c)\cos\theta(1/\tau_s-1/\tau) . \tag{15}$$

In contrast, surface-state absorption requires the modification of both $\omega_p\rightarrow\omega_p^s$ and $\tau\rightarrow\tau_s$, yielding

$$\left.\frac{\Delta R}{R_0}\right|_{p\ \mathrm{pol}} = 4(d_x/c)(1/\cos\theta)(\omega_p^s/\omega_p)^2(1/\tau_s-1/\tau) , \tag{16}$$

$$\left.\frac{\Delta R}{R_0}\right|_{s\ \mathrm{pol}} = 4(d_y/c)(\cos\theta)(\omega_p^s/\omega_p)^2(1/\tau_s-1/\tau) . \tag{17}$$

We now discuss the data in light of the above description.

2. *Electron-scattering mechanisms*

Using surface-electromagnetic-wave spectroscopy (SEWS), Riffe and co-workers[42] have studied the surface-electronic absorption of the H/W(100) system. They have argued that, above 0.42 ML, the variations of the SEW absorption coefficient are due to reconstruction-induced changes in free-carrier scattering (FCS) from the surface. Specifically, among the three possible mechanisms (electron-electron, electron-phonon, and electron-surface collisions) affecting the electron-scattering rate they contend that changes in specularity of the *electron-surface collisions* dominate the observed absorption behavior. They use their data to estimate the factor $1/\tau_s-1/\tau$ in the 1000-cm^{-1} region in terms of the Fuch's specularity parameter p, where $p=1$ for specular and $p=0$ for diffuse scattering,[58–60] according to the heuristic equation[42]

$$1/\tau_s-1/\tau\sim[0.253+6.3\times10^{-5}(\tilde{\nu}-1000)](-\Delta p) . \tag{18}$$

This equation indicates that an increase of only electron-surface collisions between phases A and B will make the reflectance ratio $[R(A)]/[R(B)]$ decrease slightly as the frequency increases. That is, for a decrease in specularity $-\Delta p>0$, the absorption $\Delta R/R_0$ should increase slightly with frequency. Such a behavior is not seen in the reflectance data, $[R(1\times1)]/R[Ic(2\times2)]$ for W(100) and $[R(1\times1)]/[R(z\times2)]$ for Mo(100), shown in Fig. 9, however. While such a decrease in reflectance occurs in the restricted 900–1100-cm^{-1} frequency region for W(100), as observed by Riffe and co-workers,[42] the higher spectral range (>1100 cm^{-1}) is characterized by a *strong* increase in reflectance with frequency. Therefore, the frequency dependence of the absorption associated with the saturated (1×1) phases is qualitatively and quantitatively inconsistent with that expected for a pure FCS mechanism and is instead attributed to surface-state absorption, as discussed in Sec. V E 3.

Before discussing the surface-state absorption, we note that there is a coverage region on W(100) for which the FCS mechanism may indeed dominate, $1.28<\Theta<2.0$ ML. LEED studies have indicated that the surface progressively orders, i.e., a maximum disorder occurs at 1.28 ML.[7] However, ion-scattering and channeling data show that the surface is locally unreconstructed.[61] It is therefore likely that the surface states, characteristic of the H-saturated surface, are present throughout this coverage range. Although inhomogeneously broadened, the $2\nu_2$ mode appears throughout this coverage range as well, manifested through the total integrated area of the vibrational absorption.[24] Therefore, all indications are that the surface at 1.28 ML has long-range disorder, which disappears as 2.0-ML saturation coverage is reached. The difference in absorption between curves (b) and (c) of Fig. 13, i.e., the uniform decrease in surface absorption as Θ varies from 1.28 to 2.0 ML, may indicate a change of surface density of electronic states, but may also result from an increase in specular scattering as suggested by Riffe and co-workers. Indeed, neglecting changes in the surface density of states over this coverage range, the observed change in reflectance from 1.28 to 2 ML, including

the relative frequency dependence, can be accounted for by a 10% increase in specularity [$\Delta p = +0.1$ in Eq. (18)]. This is a very reasonable magnitude. The lack of temperature dependence in the change in absorption between those two phases from $T=165$ to 300 K, reported by Riffe and co-workers, is also consistent with this mechanism.

3. Surface-state absorption

a. The clean W(100) surface. The large absorption associated with the clean W(100) surface and shown in Fig. 8 is attributed to the optical excitation of surface states. As pointed out by Riffe and co-workers, the FCS mechanism, modeled by Eqs. (16) and (18), cannot account for the data. On the other hand, surface-state absorption can be modeled by Eq. (16), where the quantity ω_p^s/ω_p is a function of the density of surface states (matrix element of the optical excitation) and can therefore have the observed frequency dependence. Photoemission experiments have shown that a sharp surface state centered around 0.4 eV below E_F is completely quenched by 0.35 ML of hydrogen.[62] In particular, the $Ic(2\times2)$ phase at 0.42 ML is devoid of this intrinsic surface state. In Fig. 8 the absorption associated with the clean surface appears as a *decrease* in the reflectance $(R_{\text{clean}})/\{R[Ic(2\times2)]\}$. Assuming that most of this absorption arises from the presence of this intrinsic surface state, we see that this surface state peaks at 2900 cm^{-1} (0.36 eV) with a maximum absorption of $\Delta R/R \approx 0.7\%$ at the point labeled SS and a width $\approx 2000\ \text{cm}^{-1}$ (0.25 eV).

This absorption is attributed to electronic transitions from filled surface states previously observed in ultraviolet photoemission spectroscopy (UPS) to empty states (above E_F) of the clean surface. Its width ($\sim 2000\ \text{cm}^{-1}$) is consistent with the 0.3-eV-wide feature observed at 0.35 eV in field emission,[63] which is rather narrow for an electronic state. It suggests that such states involve primarily d electrons. Such localized electrons exhibit a small dispersion, resulting in narrow absorption profiles. Furthermore, as noted in Sec. V E 1 [Eq. (11)] for p-polarized radiation incident at $\theta \approx 85°$, only electronic transitions involving the tangential component of the electric field are excited. Consequently, the surface-state absorption must have xy or x^2-y^2 symmetry. The nature of the final state is obtained by invoking spin conservation and recognizing that ~ 0.1-eV radiation can only produce intraband transitions. The infrared absorption is therefore a result of electron-hole–pair generation within surface states of d_{xy} or $d_{x^2-y^2}$ symmetry.

First-principles calculations[64,65] and recent photoemission data[66] have considered in detail the origin of the surface states at $\bar{\Gamma}$ and along the $\bar{\Sigma}$ line. In particular, the self-consistent scalar-relativistic linear-augmented-plane-wave calculations of Mattheiss and Hamann,[65] including spin-orbit coupling, show the presence of strong surface states in the vicinity of E_F with x^2-y^2 symmetry along the $\bar{\Sigma}$ line [see Figs. 6(a) and 9(b) of Ref. 65]. The broad absorption in Fig. 8 is therefore attributed to intraband transitions associated with these $d_{x^2-y^2}$ bands.

The excitation of these intraband transitions does not occur in a specular EELS experiment. Indeed, no broad feature similar to the infrared absorption shown in Fig. 8 is present in EELS spectra of the clean W(100) surface.[11,25–29] The reason for this discrepancy is that specular EELS probes the ϵ_z component of the surface response[67] for losses both above and below the surface plane, in contrast to p-polarized SIRS, which is sensitive only to $\epsilon_{x,y}$ for absorption below the surface plane of a *metallic* (large-$|\epsilon|$) substrate. Note that grazing-incidence s-polarized reflectance spectra are 2 orders of magnitude less sensitive to the surface-electronic absorption than p-polarized spectra [Eqs. (11) and (12)], which accounts for the failure to observe the surface-state absorption in s-polarized spectra.

In summary, a strong infrared absorption arising from intraband transitions of surface states with $d_{x^2-y^2}$ symmetry appears to dominate the reflectance spectrum of clean W(100). Other processes, involving free-carrier scattering at the surface, have been ruled out mostly because they cannot account for the characteristic frequency dependence of the absorption shown in Fig. 8. The latter is, of course, a small fraction ($\sim 0.7\%$) of the total electronic absorption suffered upon reflection and dominated by bulk electron-phonon scattering within the skin-depth region.[68] However, as will be apparent in the next Sec. V E 3 *b*, it is still large compared with the magnitude of the H vibrational absorption.

b. The H-saturated W(100) and Mo(100) surfaces. The data in Fig. 9 also show an electronic absorption associated with the H-saturated W(100)-$p(1\times1)$ and M(100)-$p(1\times1)$ surfaces, as evidenced by a *decrease* in reflectivity from the $Ic(2\times2)$ to the (1×1) phase and from the $(z\times2)$ to the (1×1) phase, respectively. On W(100), the absorption is centered around 1200 cm^{-1} (0.15 eV) with an approximate width of 2000 cm^{-1} (0.25 eV) and a magnitude of $\Delta R/R \approx 0.45\%$. On Mo(100) the absorption grows as the frequency decreases with no well-defined maximum. However, in both cases the absorption is strongly frequency dependent with a peak in the excitation energy below the energy of the overtone absorption, a clear requirement for a strong breakdown of adiabaticity.[52]

This frequency dependence rules out possible contributions by free-carrier scattering, as previously invoked by Riffe and co-workers.[42] Indeed, changes in specularity ($\Delta p \neq 0$) would lead to an opposite (and much weaker) frequency dependence. Instead, the strength and frequency dependence of the absorption can be well accounted for by the presence of surface-electronic states in the vicinity of E_F at saturation. The relatively narrow width (0.25 eV) of these absorption bands is again suggestive of d states. Following the same reasoning as in Sec. V E 3 *a*, we conclude that these absorption bands involve intraband transitions for states with d_{xy} or $d_{x^2-y^2}$ symmetry. In this case, however, d_{xy} states are favored, as explained below.

Among the various theoretical calculations, the results of Richter and Wilkins[49] explicitly show the presence of surface states with d_{xy} symmetry (e.g., at $\bar{\Gamma}$ and $\bar{X}$), located in the immediate vicinity of E_F (≤ 0.1 eV). Such

states, schematically shown in Fig. 7 of Ref. 69, are not altered by H adsorption (assuming an unreconstructed surface prior to adsorption) or by H vibration within the symmetry plane (xz or yz), because they do not participate in the bonding. However, they can couple to the wag motion because the latter breaks the mirror symmetry. In contrast the bonding states, to which the symmetric (ν_1) and asymmetric (ν_3) stretch modes couple strongly, are all located well below E_F (>1 eV).

A typical test for the presence of surface states at the W(100)-$p(1\times1)$H surface is to compare the electronic absorption of the H/W(100) surface with that of O/W(100), CO/W(100), and N/W(100) surfaces. The surface states detected at H saturation are not expected to be present at saturation coverage with these chemically distinct adsorbates. The data of Riffe and co-workers on these systems (Fig. 9 of Ref. 43) show that, once the intrinsic surface state has been quenched, the absorption is independent of coverage for these other species. They also noted that the variations in absorption were smaller by a factor of 2 for these systems than for the H/W(100) system. In particular, the relative absorption of the saturated phases was smaller than for H/W(100). These observations are consistent with the present results if an additional surface-state absorption is present at H saturation, but not for O, CO, or N saturation on W(100).

With regard to the strength of the surface-state absorption, an estimate performed by Riffe and co-workers[42] is relevant. Assuming the participation of one conduction electron per W surface atom, they modeled the surface absorption with a thin layer characterized by a different plasma frequency and a similar scattering time (see Sec. V A of Ref. 42), using a three-layer model. A similar description [Eqs. (11)–(17)] for the reflectance measurements yields $\Delta R/R \sim 0.3\%$, in agreement with both the measured magnitude of the intrinsic surface state (0.7%) and the surface state at saturation (0.45%). In summary, the measured frequency dependence, width, and strength of the absorption associated with the (1×1) phase are all supporting evidence for the presence of a surface state located within 0.15 eV of E_F on W(100).

If this interpretation is valid for the Mo(100) surface as well, it appears that the Mo(100)-$p(1\times1)$H surface is characterized by a surface-state band centered within 0.12 eV of E_F. While the overall strength of this band may be equal to that of the W(100)-$p(1\times1)$H surface band, its density of states *at* 1300 cm^{-1} (i.e., at the location of the $2\nu_2$ mode) is roughly half that of W. The stronger electronic absorption by W(100) is consistent with the observation of a stronger and more asymmetric $2\nu_2$ feature as well, since the parameters of this feature are proportional to the electronic density of states for a strong breakdown of adiabaticity. The appearance of surface-state absorption on Mo(100) is directly associated with the formation of the (1×1) phase as pointed out at the end of Sec. VI E 2. This behavior is similar to that of the W(100) surface, although the latter goes through a disordered (1×1) phase characterized by both surface state and FCS (disorder-induced) absorption.

In summary, we have presented evidence that, on both H-saturated W and Mo surfaces, there is a strong surface-state absorption, probably of d_{xy} symmetry. The observation of the surface-state absorption is key to the detection of the $2\nu_2$ feature that is *only* observed for the H-saturated (1×1) phases. In fact, this feature can be viewed as an interference on top of the strong electronic absorption, arising from a *strong* coupling of the wag motion to the *sharply peaked* electronic structure. Consequently, it cannot be observed without the detection of this electronic absorption. In the generalized polarizability expression given in Eq. (4) in Sec. III, the dipole moment associated with the nuclear motion μ^i is negligible compared to that of the electronic response μ^e. However, the coupling strength, expressed as $\tilde{\nu}\tilde{\tau}$ in Eq. (4) is large, leading to a strong asymmetry (see Table I).

F. Co-adsorbed CO

Co-adsorbed CO is known to modify electronically the near surface region. The H/D and H/CO co-adsorption data are compared. For a given range of N_s(H), we have observed comparable dispersion and linewidths for the $2\nu_2$ H mode on Mo(100). Yet a greater attenuation of intensity, indicated by a nonconstant value of $(e^*/e)^2$, and asymmetry parameter is found for the H/CO data. A realistic interpretation of these results necessitates an explicit knowledge of how CO modifies the adlayer structure vicinal to H. Since the frequencies and widths of $2\nu_2$ are comparable to those for the H/D co-adsorption data over the same N_s(H) range, implying similar force constants, we shall assume that H continues to bind to the two-fold bridge site, while CO occupies randomly dispersed top sites.

One explanation for the CO-associated attenuation of $2\nu_2$, therefore, is that the steric hindrance imposed by CO reduces the mean amplitude, and effectively e^*/e, and shifts the mean frequency outside our measurement window. If this were the case, however, we would expect a grosser broadening and shift in the mean frequency than was observed for the H/D studies. Alternatively, CO does modify the near surface-electronic structure and, more specifically, the surface-electronic states of d_{xy} symmetry near the Fermi edge. Since such states have been identified for the H-saturated surface, we propose that CO reduces the availability of electronic states (discussed in Sec. V E 3 *b*) of appropriate energy and d_{xy} symmetry to couple to $2\nu_2$, resulting in an attenuation of the $2\nu_2$ apparent dynamic dipole.

Finally, we observe that specular EELS excites only surface-electronic states whose dipole moments lie normal to the surface. The Mo(100)-$p(1\times1)$H and W(100)-$p(1\times1)$H surface states of d_{xy} symmetry and ϵ_{xy} excitation are thus inaccessible to a dipole EELS measurement. Indeed, such electronic excitations are absent in all specular EELS studies. The absence of a $2\nu_2$ feature in the EELS data as well further demonstrates that the intensity of optically excited $2\nu_2$ is derived largely by interference with parallel surface states of primarily d_{xy} character.

VI. CONCLUSIONS

The Mo(100)-$p(1\times1)$H and W(100)-$p(1\times1)$H surfaces exhibit two infrared-absorption bands in the 800–4000-

cm^{-1} region involving adlayer vibrations. The symmetric stretch (ν_1) is observed at 1016 cm^{-1} on Mo(100) at $T=100$ K and at 1069 cm^{-1} on W(100) at $T=300$ K. This feature is consistent with specular EELS observations. A higher-frequency absorption, which was absent from the EELS data, has also been observed at 1302 cm^{-1} on Mo(100) and 1269 cm^{-1} on W(100) and is assigned to an interference feature on a broad electronic absorption involving the first overtone of the wag motion ($2\nu_2$). The two vibrational features exhibit markedly different line shapes. The ν_1 features are broad and of a Lorentzian form, whereas the $2\nu_2$ bands are of the derivative form, typical of a Fano absorption mechanism.

Temperature-dependent, isotopically substituted, and lower-coverage data all indicate that surface inhomogeneities do not contribute significantly to the saturation line shapes. Weak dephasing, characterized by effective low-frequency substrate dephasing channels, is evident, but does not dominate the spectral observations, except perhaps for ν_1 on W(100). Likewise, dynamical coupling appears relatively weak, except in the case of ν_1 on W(100), which narrows by 45% upon 50% D coadsorption.

The characteristic Fano shape of the $2\nu_2$ mode, representative of a discrete state interfering with a continuum, requires three parameters for a phenomenological line shape. In addition to the linewidth and frequency, an asymmetry parameter is necessary to describe the interference strength. On both Mo(100) and W(100) this asymmetry parameter is temperature insensitive, indicating that the spectral profile is dominated by nonadiabatic coupling. The relatively narrow widths of these features place lower bounds on their vibrational lifetimes at $T_1 > 0.9$ ps and $T_1 > 0.6$ ps in Mo(100) on W(100), respectively.

On both surfaces the $2\nu_2$ band absorption strength is attributed to intensity borrowing from the interference continuum channel. Isotopic substitution demonstrates that this interference is not facilitated by a spatially extended (or in-phase $Q_{\parallel} \approx 0$) mode.

The identity of the continuum responsible for nonadiabatic enhancement of $2\nu_2$ was investigated via broadband reflectivity measurements of Mo(100)/H and W(100)/H as a function of coverage. The frequency dependence of the electronic absorption made it possible to distinguish between free-carrier–scattering absorption and surface-state contributions to the broadband reflectance data. Surface-state absorption is identified on Mo(100)-$p(1\times1)$H and W(100)-$p(1\times1)$H, with mean excitation energy centered at $\sim$0.12 and 0.15 eV, respectively. The absorption in both cases is relatively narrow ($\sim$0.25 eV).

Since only tangential components of the electric field, E_x and E_y, are significant below the surface plane, we conclude that the surface states measured for both the H-saturated surfaces and clean W(100) must possess primarily parallel dipole character, an x-y symmetry. Furthermore, the relatively narrow profile of the broadband absorption is characteristic of primarily d electrons. We thus propose that the surface states possess d_{xy} symmetry. We note that parallel surface-state transitions are inaccessible to dipole EELS, thereby explaining the absence of the surface-state absorption and of the $2\nu_2$ interference feature in the dipole EELS data.

Finally, co-adsorbed CO is seen to attenuate the $2\nu_2$ feature considerably. Since CO binds to the surface by interacting with electrons of d_{xy} symmetry, we suggest that CO quenches the surface states of d_{xy} character that we observe for the H-saturated surfaces. In the absence of strong surface-state absorption, consequently, nonadiabatic coupling to $2\nu_2$ is reduced, as is the nonadiabatic enhancement of $2\nu_2$.

The Mo(100)-$p(1\times1)$H and W(100)-$p(1\times1)$H surfaces give the first example of strong breakdown of adiabaticity in which a large and strongly peaked density of electronic states leads to a strong coupling. The small-ω expansion originally used by Langreth[21,22] to evaluate the isotopic dependence, the asymmetry, and the strength of the line shape is not valid when the electronic spectral density varies rapidly near E_F.[69] In particular, the isotopic dependence reported in Table I requires a strong breakdown of adiabaticity to be accounted for.[52]

ACKNOWLEDGMENTS

The authors benefited greatly from stimulating discussions with S. Andersson, P. J. Estrup, L. C. Feldman, D. R. Hamann, D. C. Langreth, Z. Y. Zhang, D. M. Riffe, N. V. Smith, M. D. Stiles, and J. C. Tully. Technical support by E. E. Chaban is also gratefully acknowledged.

APPENDIX: MEASUREMENT ACCURACY OF ELECTRONIC ABSORPTION

In the case of W(100), for which the reflectivity could be monitored over the whole coverage region $\Theta=0$ to 2 ML, systematic studies with H and D could be performed in order to assess the accuracy of such broadband measurements. In Fig. 13, reflectance data are shown for

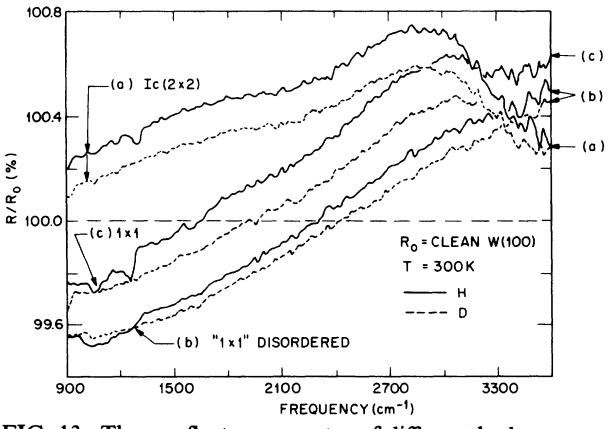

FIG. 13. Three reflectance spectra of different hydrogen- and deuterium-induced phases on W(100), referenced against the clean surface: (a) the $Ic(2\times2)$ obtained at $\Theta=0.42$ ML; (b) the (1×1) disordered phase at $\Theta=1.48$ ML; and (c) the (1×1) saturation phase. The positive peak apparent in (a) around 2900 cm^{-1} is indicative of increased absorption by the clean surface, i.e., the intrinsic surface state absorption of the clean W(100) surface at 0.36 eV. The resolution is 16 cm^{-1} and the data-acquisition time 10 s per spectrum.

both W(100)H and W(100)D, where the *clean* surface is used as a reference. Three selected phases are shown: (a) the $Ic(2\times2)$ phase where the reflectivity is highest (smallest absorption), (b) the (1×1) disordered phase obtained for $\Theta=1.48$ ML, where the reflectivity is smallest (largest absorption), and (c) the (1×1) phase at or close to saturation (4.5-L exposure).

Although the spectra associated with H and D agree well in shape, they exhibit differences in absolute magnitude. We have investigated these discrepancies in a series of runs and account for them as follows: First, for the $Ic(2\times2)$ phase the electronic absorption is a very strong function of H coverage (i.e., substrate reconstruction) and goes through a sharp minimum (Figs. 6 and 10 in Ref. 42). The difference in magnitude between H and D in curve (a) is likely due to small differences in Θ. With 10-s time resolution, we cannot monitor the coverage with better accuracy than $\Theta\sim0.05$ L, which is sufficient to account for this discrepancy. The difference in magnitude in curve (b), the smallest among the three curves, can be viewed as a typical error arising from systematic optical variations alone. Finally, the difference in curve (c) is also largely attributed to a small difference in coverage, with $\Theta(\mathrm{H})>\Theta(\mathrm{D})$. Indeed, we have observed that as the (1×1) ordered phase is developed, with the ν_1 and $2\nu_2$ vibrational features sharpening, the reflectivity keeps increasing (decreasing absorption) as the surface coverage slowly reaches saturation. Because of kinetic effects, 4.8-L D_2 exposure corresponds to 3.4-L H_2 exposure, which is not quite sufficient to establish complete saturation.[42] We conclude that the reflectivity of the (1×1) phase depends critically on the establishment of the H or D layer, which presumably affects the W reconstruction. Consequently, at saturation coverage the electronic absorption of the D-covered surface is, within our error bars, the same as that of the H-covered surface, dismissing a previous suggestion of such an isotopic electronic effect.[69]

[1]Y. J. Chabal, Surf. Sci. Rep. **8**, 211 (1988).

[2]D. R. Hamann, J. Electron. Spectrosc. Relat. Phenom. **44**, 1 (1987).

[3]P. J. Estrup and J. Anderson, J. Chem. Phys **45**, 2254 (1966).

[4]P. J. Estrup, J. Vac. Sci. Technol. **16**, 635 (1979).

[5]D. A. King and G. Thomas, Surf. Sci. **92**, 201 (1980).

[6]R. A. Barker and P. J. Estrup, Phys. Rev. Lett. **41**, 1307 (1978).

[7]R. A. Barker and P. J. Estrup, J. Chem. Phys. **74**, 1442 (1981).

[8]J. J. Arrecis, Y. J. Chabal, and S. B. Christman, Phys. Rev. B **33**, 7906 (1986).

[9]J. A. Prybyla, P. J. Estrup, and Y. J. Chabal, J. Vac. Sci. Technol. A **5**, 791 (1987).

[10]J. A. Prybyla, P. J. Estrup, S. C. Ying, Y. J. Chabal, and S. B. Christman, Phys. Rev. Lett. **58**, 1877 (1987).

[11]W. Ho, R. F. Willis, and E. W. Plummer, Phys. Rev. Lett. **40**, 1463 (1978).

[12]F. Zaera, E. B. Kollin, and J. L. Gland, Surf. Sci. **166**, L149 (1986).

[13]B. N. J. Persson and M. Persson, Surf. Sci. **97**, 109 (1980).

[14]B. N. J. Persson and S. Andersson, Phys. Rev. B **29**, 4382 (1984).

[15]B. N. J. Persson and R. Ryberg, Phys. Rev. B **32**, 3586 (1985).

[16]B. Hellsing, Surf. Sci. **152/153**, 826 (1985).

[17]J. C. Ariyasu, D. L. Mills, K. G. Lloyd, and J. C. Hemminger, Phys. Rev. B **28**, 6123 (1983); **30**, 507 (1984).

[18]A. G. Eguiluz, Phys. Rev. B **30**, 4366 (1984).

[19]J. W. Gadzuk and A. C. Luntz, Surf. Sci. **144**, 429 (1984).

[20]R. G. Tobin, Surf. Sci. **183**, 226 (1987).

[21]David C. Langreth, Phys. Rev. Lett. **54**, 126 (1985).

[22]Z. Crljen and D. C. Langreth, Phys. Rev. B **35**, 4224 (1987).

[23]Y. J. Chabal, Phys. Rev. Lett. **55**, 845 (1985).

[24]Y. J. Chabal, J. Vac. Sci. Technol. A **4**, 1324 (1986).

[25]A. Adnot and J.-D. Carette, Phys. Rev. Lett. **39**, 209 (1977).

[26]M. R. Barnes and R. F. Willis, Phys. Rev. Lett. **41**, 1729 (1978).

[27]J. P. Woods and J. L. Erskine, Phys. Rev. Lett. **55**, 2595 (1985).

[28]J. P. Woods and J. L. Erskine, J. Vac. Sci. Technol. A **4**, 1414 (1986).

[29]J. L. Erskine, J. P. Woods, A. D. Kulkarni, and F. W. de Wette, J. Electron. Spectrosc. Relat. Phenom. **44**, 27 (1987).

[30]H. Ibach, Surf. Sci. **66**, 56 (1977). Note that all reported values of e^*/e are too low by a factor of $\sqrt{2}$ as explained in A.M. Barro, H. Ibach, and H. D. Bruchmann, Surf. Sci. **88**, 384 (1979).

[31]L. H. Dubois, G. P. Schwartz, R. E. Camley, and D. L. Mills, Phys. Rev. B **29**, 3208 (1984).

[32]We would like to thank Professor P. J. Estrup for providing us the Mo(100) sample which was also used in the work reported in Refs. 9 and 10.

[33]J. A. Prybyla, P. J. Estrup, Y. J. Chabal, and S. B. Christman (unpublished).

[34]For free-carrier–scattering mechanisms, the measured $\Delta R/R$ is roughly proportional to $1/\tau$ [see Eq. (14)], i.e., proportional to ρ, the metal conductivity. The conductivity varies from 0.85 to 4.95 $\mu\Omega$ cm between $T=100$ and 300 K for tungsten [Kannuluik, Proc. R. Soc. London **141**, 159 (1933)]. In general, the temperature dependence is therefore stronger than linear for the temperature range under investigation.

[35]U. Fano, Phys. Rev. **124**, 1866 (1961).

[36]D. M. Riffe, L. M. Hanssen, A. J. Sievers, Y. J. Chabal, and S. B. Christman, Surf. Sci. **151**, L559 (1985).

[37]A. Horlacher Smith, R. A. Barker, and P. J. Estrup, Surf. Sci. **136**, 327 (1984).

[38]B. Banse, K. G. Lloyd, and J. C. Hemminger, J. Chem. Phys. **86**, 2986 (1987).

[39]A. S. Barker, Jr. and A. J. Sievers, Rev. Mod. Phys. **47**, S1 (1975).

[40]J. Anderson, G. W. Rubloff, M. A. Passler, and P. J. Stiles, Phys. Rev. B **10**, 2401 (1974).

[41]J. B. Restorff and H. D. Drew, Surf. Sci. **88**, 399 (1979).

[42]D. M. Riffe, L. M. Hanssen, and A. J. Sievers, Phys. Rev. B **34**, 692 (1986).

[43]D. M. Riffe, L. M. Hanssen, and A. J. Sievers, Surf. Sci. **176**, 679 (1986).

[44]See, for instance, Shen-Shu Sung, and Roald Hoffman, J. Am. Chem. Soc. **107**, 578 (1985).

[45]F. Zaera, E. Kollin, and J. L. Gland, Chem. Phys. Lett. **121**,

464 (1985).
[46]H. Ibach and D. L. Mills, *Electron Energy Loss Spectroscopy and Surface Vibrations* (Academic, New York, 1982), p. 188.
[47]S. H. Chen, Ph.D. thesis, McMaster University, 1964 (unpublished).
[48]R. S. Sorbello, Phys. Rev. B **32**, 6924 (1985).
[49]R. Richter and J. W. Wilkins, Surf. Sci. **128**, L190 (1983).
[50]R. Biswas and D. R. Hamann, Phys. Rev. Lett. **56**, 2291 (1986).
[51]M. Weinert, A. J. Freeman, and S. Ohnishi, Phys. Rev. Lett. **56**, 2295 (1986).
[52]Z. Y. Zhang and D. C. Langreth (unpublished).
[53]N. J. Harrick, *Internal Reflection Spectroscopy* (Wiley, New York, 1967) [Revised edition: (Harrick Scientific, Ossining, NY, 1979), pp. 76–81].
[54]B. N. J. Persson and R. Ryberg, Phys. Rev. Lett. **54**, 2119 (1985).
[55]H. Morawitz, Phys. Rev. Lett. **58**, 2778 (1987).
[56]C. M. Mate and G. A. Somorjai, Phys. Rev. B **34**, 7417 (1986).
[57]See Table 3 of Ref. 1 and references therein. Also, C. M. Mate, B. E. Bent, and G. A. Somorjai, in *Hydrogen in Catalysis—Theoretical and Practical Aspects,* edited by Z. Paal (Dekker, New York, 1986).
[58]T. Holstein, Phys. Rev. **88**, 1427 (1952).
[59]R. B. Dingle, Physica **19**, 311 (1953); **19**, 729 (1953).
[60]K. Fuchs, Proc. Cambridge Philos. Soc. **34**, 100 (1938).
[61]I. Stensgaard, L. C. Feldman, and P. J. Silverman, Phys. Rev. Lett. **42**, 247 (1979); L. C. Feldman, P. J. Silverman, and I. Stensgaard, Surf. Sci. **87**, 410 (1979).
[62]E. W. Plummer and R. D. Young, Phys. Rev. B **1**, 2088 (1970); B. J. Waclawski and E. W. Plummer, Phys. Rev. Lett. **29**, 783 (1972); B. Feuerbacher and B. Fitton, *ibid.* **29**, 786 (1972).
[63]L. W. Swanson and L. C. Crouser, Phys. Rev. Lett. **16**, 389 (1966); Phys. Rev. **163**, 622 (1967).
[64]M. Posternak, H. Krakauer, A. J. Freeman, and D. D. Koelling, Phys. Rev. B **21**, 5601 (1980).
[65]L. F. Mattheiss and D. R. Hamann, Phys. Rev. B **29**, 5372 (1984).
[66]S.-L. Weng, E. W. Plummer, and T. Gustafsson, Phys. Rev. B **18**, 1718 (1978); J. C. Campuzano, D. A. King, C. Somerton, and J. E. Inglesfield, Phys. Rev. Lett. **45**, 1649 (1980); **47**, 443 (1981); M. I. Holmes and T. Gustafsson, *ibid.* **47**, 443 (1981).
[67]*Electron Energy Loss Spectroscopy and Surface Vibrations,* Ref. 46, pp. 76–101.
[68]F. J. Blatt, *Physics of Electronic Conduction in Solids* (McGraw-Hill, New York, 1968), pp. 183–196.
[69]Y. J. Chabal, J. Electron. Spectrosc. Relat. Phenom. **38**, 159 (1986).